# AXIAL BUCKLING LOAD OF PARTIALLY ENCASED COLUMNS UNDER FIRE

**ABDELKADIR FELLOUH**

Final thesis presented to

**School of Technology and Management**

**Polytechnic Institute of Bragança**

For the fulfilment of the Master degree in

**CONSTRUCTION ENGINEERING**

**July 2016**

This page was intentionally left in blank

# AXIAL BUCKLING LOAD OF PARTIALLY ENCASED COLUMNS UNDER FIRE

**ABDELKADIR FELLOUH**

Final thesis presented to

**School of Technology and Management**

**Polytechnic Institute of Bragança**

For the fulfilment of the Master degree in

**CONSTRUCTION ENGINEERING**

Supervisor at IPB:

**Prof. Paulo Piloto**

Supervisor at UHBC**:**

**Prof. Nourredine Benlakehal**

**July 2016**

This page was intentionally left in blank

**ACKNOWLEDGEMENTS**

My thanks go especially to my parents who supported me from the beginning. I also thank the supervisors of the thesis, Dr. Paulo Piloto, coordinator Professor from the Department of Applied Mechanics, School of Technology and Management, Polytechnic Institute of Bragança, and Dr. Nourredine Benlakehal, Department of Civil Engineering, Faculty of Civil Engineering and Architecture, University Hassiba Benbouali of Chlef.

I thank all my professors especially from IPB Dr. Luís Mesquita and Dra. Elza Fonseca and from UHBC Dr Lamri Belkacem and Dr. kada Abdelhak for helping, support and encouragement.

I thank the School of Technology and Management of the IPB for the use of facilities and equipment, in particular the Prof. Dr. Rufino Amaro. Finally, thank the support of family, friends, and colleagues.

This page was intentionally left in blank

## ABSTRACT

Partially encased columns have significant fire resistant. However, it is not possible to assess the fire resistance of such members simply by considering the temperature of the steel. The presence of concrete increases the mass and thermal inertia of the member and the variation of temperature within the cross section, in both the steel and concrete components. The annex G of EN1994-1-2 allows to calculate the load carrying capacity of partially encased columns, for a specific fire rating time, considering the balanced summation method. New formulas will be used to calculate the plastic resistance to axial compression and the effective flexural stiffness. These two parameters are used to calculate the buckling resistance. The finite element method is used to compare the results of the elastic critical load for different fire ratings of 30 and 60 minutes. The buckling resistance is also calculated by the finite element method, using an incremental and iterative procedure. This buckling resistance is also compared with the simple calculation method, evaluating the design buckling curve that best fits the results.

## KEYWORDS

Partially encased column; Fire resistance; Simplified and advanced calculation methods; Buckling.

This page was intentionally left in blank

**RESUMO**

As colunas parcialmente embebidas com betão possuem elevada resistência ao fogo. No entanto, não é possível avaliar a resistência ao fogo de tais elementos simplesmente considerando a evolução da temperatura do aço. A presença de betão aumenta a massa, a inércia térmica do elemento e a variação de temperatura dentro da seção transversal, tanto no aço como nos componentes de betão. O anexo G da EN1994-1-2 permite calcular a capacidade resistente de colunas parcialmente embebidas com betão, para um tempo específico resistência ao fogo, considerando o método da soma pesada das componentes. Novas fórmulas serão utilizadas para calcular a resistência plástica à compressão axial e a rigidez à flexão efetiva. Estes dois parâmetros são utilizados para calcular a resistência à encurvadura. O método dos elementos finitos é utilizado para comparar os resultados da carga crítica elástica para diferentes classificações de resistência ao fogo, 30 e 60 minutos. A resistência à encurvadura também é calculada pelo método dos elementos finitos, por um processo incremental e iterativo. A resistência à encurvadura é também comparada com o método de cálculo simplificado, avaliando a curva de encurvadura que melhor se ajusta aos resultados.

**PALAVRAS CHAVE**

Colunas parcialmente embebidas com betão; Resistência ao fogo; Método simplificado e avançado de cálculo; Encurvadura.

**INDEX**

**ANNEX**

## LIST OF FIGURES

## LIST OF TABLES

## NOTATIONS

### Latin upper case letters

| | |
|---|---|
| $A_c$ | Cross-sectional area of the concrete. |
| $A_s$ | Cross-sectional area of the reinforcement. |
| $A_m/V$ | Section factor. |
| $E$ | Modulus of elasticity. |
| $E_a$ | Modulus of elasticity of the structural steel at room temperature. |
| $E_{a,\theta}$ | Modulus of elasticity of the structural steel at elevated temperature. |
| $E_c$ | Effective modulus of elasticity of the concrete at room temperature. |
| $E_{cm}$ | Secant modulus of elasticity of the concrete at room temperature. |
| $E_{c,\sec,\theta}$ | Characteristic value for the secant modulus of concrete in the fire situation. |
| $(EI)_{fi,c,z}$ | Effective flexural stiffness of the concrete around the z-axis exposed to fire |
| $(EI)_{fi,eff,z}$ | Effective flexural stiffness of a composite section around the z-axis exposed to fire. |
| $(EI)_{fi,f,z}$ | Effective flexural stiffness of the flange around the z-axis exposed to fire. |
| $(EI)_{fi,w,z}$ | Effective flexural stiffness of the web around the z-axis exposed to fire. |
| $(EI)_{fi,s,z}$ | Effective flexural stiffness of the reinforcement around the z-axis exposed to fire. |
| $E_s$ | Modulus of elasticity of the steel reinforcement at room temperature. |
| $E_{s,\theta}$ | Characteristic value for the slope of the linear elastic range of the stress-strain relationship of reinforcing steel at elevated temperatures. |
| $H_t$ | Factor. |
| $I_y$ | Moment of inertia relative to the axis y-y. |
| $I_z$ | Moment of inertia relative to the axis z-z. |

| | |
|---|---|
| $Q_c$ | Is the convective part of the rate of heat release. |
| $[K]$ | The element stiffness matrix. |
| $[S]$ | Geometric stiffness matrix of the element. |
| $L$ | Length of the column. |
| $L_{cr}$ | Buckling length. |
| $N_{fi,cr,z}$ | Elastic critical load (≡ Euler buckling load) around the axis Z in the fire situation. |
| $N_{fi,pl,Rd}$ | Normal plastic stress resistant exposed to fire. |
| $N_{fi,b,Rd}$ | Buckling resistant exposed to fire. |
| $T, \theta$ | Temperature. |
| $W_{pl}$ | Plastic section modulus. |

**Latin lower case letters**

| | |
|---|---|
| $b$ | Width of the cross section. |
| $b_w$ | Width of the web element. |
| $b_{c,fi}$ | Neglected external layer of concrete. |
| $b_{c,fi,horizontal}$ | Neglected external layer of concrete in horizontal directions. |
| $b_{c,fi,vertical}$ | Neglected external layer of concrete in vertical directions. |
| $c_a(\theta)$ | Specific heat of steel. |
| $c_p(\theta)$ | Specific heat of concrete. |
| $f_{cd}$ | Design value of the yield strength of the steel at room temperature. |
| $f_{cm}$ | The average design value of the yield strength of the steel at room temperature. |
| $f_{sk}$ | Characteristic value of the yield strength of the steel reinforcement at room temperature |
| $f_{ck}$ | Characteristic value of the compressive strength of the concrete at room Temperature. |

| | |
|---|---|
| $f_{u,\theta}$ | The ultimate strength at elevated temperature, allowing for strain-hardening. |
| $h$ | Total height of a cross section. |
| $h_1$ | Height between web. |
| $\dot{h}_{net}$ | Net heat flow per unit area. |
| $\dot{h}_{net,c}$ | Net convective heat flux per unit surface area. |
| $\dot{h}_{net,d}$ | Design value of the density of heat flow per unit area. |
| $\dot{h}_{net,r}$ | Net radioactive heat flux per unit surface area. |
| $h_{w,fi}$ | Height reduction of the web. |
| $k_{E,\theta}$ | Reduction factor for the slope of linear elastic range at the steel temperature $\theta_a$ reached at time t. |
| $k_{c\theta}$ | Reduction factor for the tensile strength of concrete. |
| $k_{p,\theta}$ | Reduction factor of the yield point of structural steel giving the proportional limit at temperature $\theta_a$ reached at time t. |
| $k_{y,\theta}$ | Reduction factor for effective yield strength at the steel temperature $\theta_a$ reached at time t. |
| $t$ | Time. |
| $t_f$ | Flange thickness. |
| $t_w$ | Web thickness. |
| $u$ | Geometric mean of the distances $u_1$ $u_2$ . |
| $u_1$ $u_2$ | Shortest distance between the reinforcing steel centre and inner face of the flange or the nearest end of concrete. |
| $z$ | Height along the flame axis. |

**Greek upper case letters**

| | |
|---|---|
| $\nabla\theta$ | $\nabla\theta = \langle d\theta/d_x \quad d\theta/d_y \quad d\theta/d_z \rangle^t$ |
| $\phi$ | Configuration factor. |
| $\phi_{LT}$ | Value to determine the reduction factor $\chi_{LT}$ . |

| | |
|---|---|
| $\phi_{LT,\theta,com}$ | Value to determine the reduction factor $\chi_{LT}$ at elevated temperature $\theta$. |

**Greek lower case letters**

| | |
|---|---|
| $\alpha$ | Imperfection factor, thermal elongation coefficient. |
| $\alpha_c$ | Coefficient of heat transfer by convection. |
| $\beta$ | Parameters to take into account the effect of biaxial bending. |
| $\varepsilon$ | Emissivity of material. |
| $\varepsilon_{c,\theta}$ | Thermal strain of concrete. |
| $\varepsilon_{p,\theta}$ | Thermal strain of pressurising steel. |
| $\varepsilon_{s,\theta}$ | Thermal strain of reinforcing steel. |
| $\varepsilon_f$ | Emissivity of the fire. |
| $\varepsilon_m$ | Surface emissivity of the member. |
| $\eta_{fi,t}$ | Amplitude charging for fire resistance calculation. |
| $\theta_a$ | Temperature of steel profile [°C]. |
| $\theta_c$ | Temperature of concrete [°C]. |
| $\theta_s$ | Temperature of reinforcement [°C]. |
| $\theta_g$ | Gas temperature in the vicinity of the element or in the fire compartment. |
| $\theta_r$ | Effective radiation temperature of the fire environment. |
| $\theta_{c,t}$ | Average temperature in the concrete at time t. |
| $\theta_{f,c}$ | Average temperature in the flange at time t. |
| $\theta_{w,c}$ | Average temperature in the web at time t. |
| $\theta_{s,c}$ | Average temperature in the reinforcement at time t. |
| $\lambda_a$ | Thermal conductivity of steel. |

| | |
|---|---|
| $\lambda_c$ | Thermal conductivity of concrete. |
| $\lambda_{(\theta)}$ | Thermal conductivity. |
| $\overline{\lambda}_{LT}$ | Relative slenderness for lateral torsional bending. |
| $\rho$ | Density. |
| $\nu$ | Poisson coefficient in elastic regime. |
| $\sigma$ | Stefan Boltzmann constant. |
| $\sigma_x$ | Principal stress in the x direction. |
| $\chi_{LT}$ | Reduction factor for lateral torsional buckling. |
| $\chi_{LT,fi}$ | Reduction factor for buckling torsional lateral sections exposed to fire. |

This page was intentionally left in blank

# CHAPTER.1 INTRODUCTION

## 1-1- Objective and motivation

The main objective is to determine the buckling load of partially encased columns (PEC) under fire, using two different methods (simple calculation method and advanced calculation methods), and also to assess the global three dimensional behaviour of PEC.

The study proposes a new formulae for the calculation method of the plastic resistance to axial compression and for the calculation method of the effective flexural stiffness of partially encased sections using the contribution of the four components of the cross sections, and a comparison is made with the simplified calculation method proposed in the standard EN1994-1-2 [1].

The advanced calculation method is based on a four step calculation process. The first step solves the nonlinear transient thermal analysis to define the temperature of the elements under fire. The second step considers a static and Eigen buckling analysis to define the elastic buckling resistance for specific fire rating periods (30 and 60 minutes). The third step considers the nonlinear incremental solution method to find the plastic resistance of the cross section for specific fire rating periods (30 and 60 minutes). The fourth and finally step considers the nonlinear incremental solution method to find the buckling resistance of partially encased columns for specific fire rating periods (30 and 60 minutes).

The thermal analysis is very important to define the thermal effect on the mechanical properties of three different materials (steel, concrete and reinforcement). Specific temperature fields are applied to the four components of partially encased columns, corresponding to the end of each fire rating period.

The static linear analysis is the basis for the eigen buckling analysis. The solution must be found primarily, assuming an arbitrary load on the partially encased column (usually a unit force). The numerical solution of a linear buckling analysis assumes that everything is perfect and therefore the real buckling load will be lower than the calculated buckling load if the imperfections are taking into account.

A similar three dimensional model was defined to calculate the plastic resistance but using the geometrical and material nonlinear analysis. This simulation is based on

the incremental displacement in vertical direction and iterative solution method (Newton Raphson) to evaluate the value of plastic resistance.

To determine the buckling resistance, a similar three dimensional model was defined, but using the buckling mode obtained from the second step (eigen buckling analysis) to reproduce the geometric imperfection, according to standards [2]. This solution method is based on the incremental displacement and iterative solution methods (Newton Raphson).

Partially Encased Columns (PEC) are composite elements with specific features that presents some advantages with respects to other material solutions. These elements are considerably stronger than simple steel column, and (PEC) with smaller sections can be used when compared to reinforced concrete columns. One of the weaknesses is related to fire behaviour, so there is a need and interest in defining (PEC) behaviour in these conditions. The results of this study are intended to formulate new proposals for simplified calculation methods and the validation of the numerical models.

### 1-2- Fire safety

Fire has always been a very destructive natural and accidental phenomenon. The fire risk will always exist because of fire accidents and also it is impossible to use only incombustible products in building.

The primary goal of fire protection is to limit the probability of death and minimise the property losing in an unwanted fire. The most common objective in providing life safety is to ensure safe escape by giving time to people before the collapse of building. To do this, it is necessary to use more fire-resistant materials in construction and protect the structural elements, finally it is important to alert people to provide suitable escape paths and ensure that they are not affected by fire or smoke while escaping through those paths to a safe place.

According to Portuguese regulation [3] and depending on the type of structural elements, buildings must have a fire resistance to ensure its load bearing capacity (R), integrity (E) and insulation (I). The load bearing capacity is the time in completed minutes for which the test specimen continues to maintain its ability to support the test load during the test satisfying a well-defined performance criteria. The integrity, the time in completed minutes for which the test specimen continues to maintain its

separating function during the test without letting flames go through the specimen satisfying a well-defined performance criterion. The insulation is the time in completed minutes for which the test specimen continues to maintain its separating function during the test without developing temperatures on its unexposed surface satisfying a well-defined performance criterion. These criteria can be represented graphically in Fig. 1

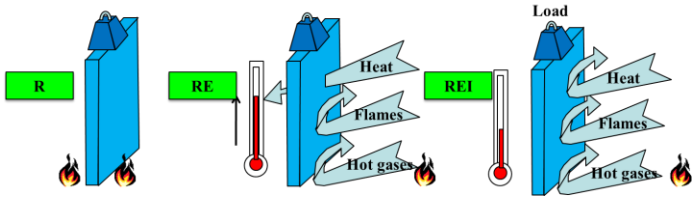


Fig. 1 - Definition of risk class.

Table 1 presents the fire rating for each building class (I to XII) and risk class (1st to 4th)

Table 1 - Minimum fire ratings for structural elements of buildings.

| CLASS OF BUILDING | RISK CLASS | | | | ELEMENT TYPE |
|---|---|---|---|---|---|
| | 1ª | 2ª | 3ª | 4ª | |
| I, III, IV, V, VI, VII,VIII, IX, X | R30 | R60 | R90 | R120 | SUPPORT |
| | REI30 | REI60 | REI90 | REI120 | SUPPORT AND PARTITIONING |
| II, XI, XII | R60 | R90 | R120 | R180 | SUPPORT |
| | REI60 | REI90 | REI120 | REI180 | SUPPORT AND PARTITIONING |

Where the class of building is define as: Type I stands for residential; Type II stands for parking places; Type III stands for business buildings; Type IV stands for schools; Type V stands for hospitals and elderly homes; Type VI stands for public shows and meetings; Type VII stands for hotels and restaurants; Type VIII stands for commercial and transport station; Type IX stands for sports and leisure; Type X stands for museums and art galleries; Type XI stands for libraries and archives and finally Type XII stands for industrial and warehouse.

Where the risk class of building depends on the height of the building and on the number of floors below reference level, see Table 2 and Fig. 2.

Table 2 - Risk building category.

| RISK BUILDING CATEGORY | height of buildings h | Number floors below reference n |
|---|---|---|
| 1. <= | 9 | 1 |
| 2. <= | 28 | 3 |
| 3. <= | 50 | 5 |
| 4. <= | 50 | 5 |

Fig. 2 present an explanation of height of building and reference level.

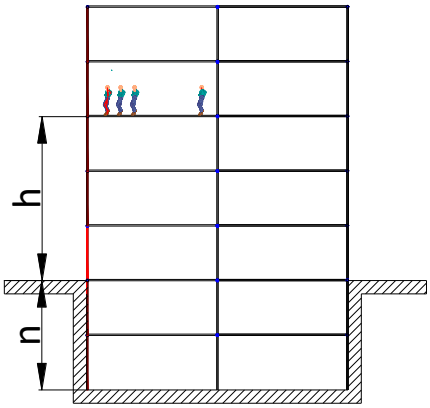


Fig. 2 - Height of building h and reference level.

### 1-3- Organization of the thesis

The thesis is organised in seven chapters. In the following paragraphs, a brief description of the contents of each is presented.

Chapter 1 is an introduction to the research work presented in this thesis, where the objective and motivation is presented. The state of the art is also included.

Chapter 2 presents the Partially Encased Columns (PEC), with a definition of the mechanical and thermal properties of materials. The fire curves and thermal actions are also explained.

In chapter 3, the simple calculation method is presented and applied to (PEC) when submitted to fire by four sides. This method is based on the weighted summation of four components, according to EN1994-1-2 [1] to determine the buckling resistance of PEC under standard fire ISO834 [4]. The effective flexural stiffness around the weak axis and the plastic resistance of the cross section, are the most important parameters to be calculated.

Chapter 4 presents new formulas to be used for the balanced summation method of ANNEX G used to calculate the plastic resistance to axial compression and the effective flexural stiffness. These two parameters are used to calculate the buckling resistance of the columns.

Chapter 5 presents the advanced calculation method for the analysis of the axial buckling Load and the plastic resistance of PEC. Numerical simulations use the finite element ANSYS software with an uncoupled thermal and mechanical analysis.

Chapter 6 presents the results of the advanced calculation method which are compared with the results from new proposed formulae for the simplified method of Eurocode EN1994-1-2 [1].

Chapter 7 presents the main conclusions and proposals for future work.

### 1-4- State of the art

Partially Encased Columns are usually made of hot rolled steel profiles, reinforced with concrete between the flanges. The composite section is responsible for increasing the torsional and bending stiffness when compared to the same section of the steel profile. In addition to these advantages, the reinforced concrete is responsible for increasing the fire resistance.

Partially Encased Columns have significant fire resistant. However, it is not possible to assess the fire resistance of such members simply be considering the temperature of the steel. The presence of concrete increases the mass and thermal inertia of the member and the variation of temperatures within the cross section, in both the steel and concrete components. The annex G of EN1994-1-2 [1] allows calculating the load carrying capacity of Partially Encased Columns, for a specific fire rating time, considering the balanced summation method.

The behaviour of composite columns made of partially encased steel sections subjected to fire has been numerically investigated by several authors, especially in this decade, but even so only a few experimental studies have been published on these types of columns with restrained thermal elongation. The major part of the experimental studies published until now is on hollow steel columns.

In 1964 Malhotra and Stevens [5] presented the results of fourteen fire resistance tests on totally encased steel stanchions with free thermal elongation, The results show

that the concrete cover has a significant effect on the fire resistance, and the lightweight concrete has higher fire resistance compared to normal gravel concrete which has more spalling. Given the fact that the load level is known to play a very important role in the fire resistance of columns.

In 1987, J. B. Schleich [6] was the project leader of an important experimental and numerical campaign developed to test and analyse the behaviour of Partially Encased Columns (PEC) and Beams (PEB) with and without connection to the slab. This project demonstrated the possibilities of the computer code CEFICOSS- which means "Computer Engineering of the Fire resistance for Composite and Steel Structures", able to cover most structural fire applications. This programme CEFICOSS has to be considered as a general thermo-mechanical numerical Computer code allowing to predict the behaviour under fire conditions of structural building parts such as columns, beams or frames. These structural elements could be composed either of bare steel profiles or of steel sections protected by any insulation, either of any composite cross-section type.

Karl Kordina [7] presented tables to be used as fire design guides, based on experiments. These results were verified in PEC and PEB, for certain degree of utilization, supporting conditions and materials.

In 1990 Lie and Chabot [8] tested five concrete-filled circular hollow columns and proposed a mathematical model to predict the temperature distribution within the cross-section and the structural response to fire. The heat transfer analysis is based on a division of the circular section into annular elements, while gas temperature around the section was considered uniform. The effect of moisture in the concrete was considered, by assuming that when an element within the cross section reaches the temperature of 100ºC or above, all the heating to that element drives out moisture until it is dry. This mathematical model was later applied to composite steel-concrete columns with rectangular cross-section and circular composite columns with fiber-reinforced concrete. The same authors presented another study in 1996 on the behaviour of fiber-reinforced concrete-filled hollow columns. The benefits of this type of concrete on the fire resistance of the columns were compared with those of the plain and bar-reinforced concrete.

In 2000 Stefan Winter and Jörg Lange [9] present tests on partially encased columns using high-strength steel. Special emphasis was laid on strength tests of high-tensile-steel under fire condition because the steel of the flanges would be directly

exposed to high temperatures in the event of a fire. With the currently available data it is not possible to give exact proof of the reliability of the design formulae of the German codes for high strength steel in Partially Encased Composite Columns. Furthermore the extreme weakening of the yield strength under high temperatures severely reduces the efficiency of these columns.

In 2002 Han et al [10] carried out six compressive strength tests on protected and unprotected concrete-filled rectangular hollow columns, after exposure to the ISO 834 fire curve. The unprotected columns were heated in a fire resistance furnace for 90 min while the fire protected ones were heated for 180 min. After cooling down the columns were compressed with centred or eccentric loading in order to determine their residual buckling strength.

In 2006, Brent Pricket and Robert Driver [11] developed a research project to study the behaviour of Partially Encased Columns soaked with normal concrete and high performance concrete. They concluded that the collapse of the columns with high performance concrete took place in a sudden manner compared to normal concrete columns. The ultimate behaviour of high performance columns reinforced with steel fibres was ductile. They also concluded that the bending around the stronger axis reached to the last tensions in the steel but the bending around the weak axis is reached the ultimate stresses in the concrete. This behaviour is justified by the confinement of concrete by fibre profile uprights when subjected to bending around the strong axis.

In 2010 António J.P. Moura Correia and João Paulo C. Rodrigues [12] present the results of a series of fire resistance tests in PEC with restrained thermal elongation. A new experimental set-up, specially conceived for fire resistance tests on building columns, was used for these tests. The experimental set-up was conceived so that the axial and rotational restraint of the columns would be similar to the conditions in a real building. The parameters studied were the load level, the axial and rotational restraint ratios and the slenderness of the PEC. The main conclusion of this work is that for low load levels the stiffness of the surrounding structure has a major influence on the behaviour of the column subjected to fire. Increasing the stiffness of the surrounding structure led to reductions in the critical times. The same behaviour was not observed for the higher load levels.

In 2013 Shan-Shan Huang, Buick Davison, Ian W. Burgess [13] presents a paper reports on a series of tests at elevated temperatures on connections between steel beams and H-section columns, both unfilled and partially-concrete-encased. Reverse-channel

connections to both types of column, as well as flush endplate connections to partially-encased H-section columns, were studied. The experiments aimed to investigate the behaviour of beam-to-column connections subject to significant tying forces and large rotations in fire situations, and to provide test data for development and validation of simplified component-based connection models. It has been found that reverse-channel connections provide not only high strength, but also the high ductility which is required to reduce the possibility of connection fracture and to improve the robustness of buildings in fire.

In 2013, Paulo A.G. Piloto et al. [14] conducted an experimental investigation using partially encased beams to test its fire resistance and found that the beams attained the ultimate limit state by lateral torsional buckling mode. The results show the dependence of the fire resistance on the load level. The results for critical temperature are also presented. The results have provided essential data to the calibration and validation of new simplified design methods, tabulated data and advanced numerical methods.

In 2014 Sadaoui Arezki, Illouli Said [15] presented a practical method based on Campus-Massonet criteria which was initially developed to steel structures with combined compression and bending, and also adapted for the calculation of the buckling resistance of eccentrically loaded PEC.

# CHAPTER.2 COLUMN UNDER FIRE

## 2-1- Fire curves

### 2-1-1- Nominal fire curves

The Standard temperature-time curve ISO 834 [4], also known as the Cellulosic curve and/or the standard nominal fire curve, is used as test method for determining the fire resistance of various elements of construction when subjected to standard fire exposure conditions. The test data thus obtained will permit subsequent classification on the basis of the duration for which the performance of the tested elements under these conditions satisfies specified criteria.

In 1981, Margaret Law [16] presented a paper at the ASCE Spring Convention in New York entitled "Designing fire safety for steel – recent work", the visionary paper presented a summary of novel work that she and her colleagues at Arup Fire had completed to evaluate the structural fire safety of innovative and architecturally exciting buildings – such as the Pompidou Centre in Paris. Among the many topics covered in this paper, stated a number of criticisms of the standard fire resistance test and proposed the way forward using knowledge-based analytical approaches.

The standard temperature-time curve is not representative of a real fire in a real building. Indeed it is physically unrealistic and actually contradicts knowledge from fire dynamics. The standard temperature-time curve is given according to next expression.

$$\theta_g = 20 + 345\log_{10}(8t + 1) \quad [°C] \tag{1}$$

Where $\theta_g$ is the gas temperature in the fire compartment [°C], t is the time [min], assuming the coefficient of heat transfer by convection equal to $\alpha_c = 25 \ \left[W / m^2 K\right]$.

The external fire curve is intended for the outside of separating external walls which are exposed to the external plume of a fire coming either from the inside of the respective fire compartment, from a compartment situated below or adjacent to the respective external wall. This curve is not to be used for the design of external steel structures for which a specific model exists. The external fire curve is given by:

$$\theta_g = 20 + 660.\left(1 - 0{,}687.e^{-0{,}32.t} - 0{,}675.e^{-0{,}38.t}\right) \ [°C] \tag{2}$$

Where $\theta_g$ is the gas temperature in the fire compartment [°C], t is the time [min] and the coefficient of heat transfer by convection is consider equal to $\alpha_c = 25 \ [W/m^2K]$.

The hydrocarbon is a nominal temperature-time curve used in case where storage of hydrocarbon materials makes fires extremely severe, the hydrocarbon temperature-time curve is given by:

$$\theta_g = 20 + 1080.\left(1 - 0{,}325.e^{-0{,}167.t} - 0{,}675.e^{-2{,}5.t}\right) \ [°C] \tag{3}$$

Where $\theta_g$ is the gas temperature in the fire compartment [°C], t is the time [min] and the coefficient of heat transfer by convection is consider equal to $\alpha_c = 50 \ [W/m^2K]$ Fig. 3 represents the variation of the gas temperature versus time for the nominal fire curves.

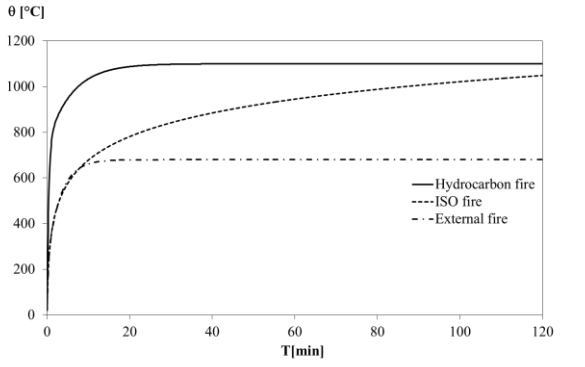


Fig. 3 - Nominal fire curves.

### 2-1-2- Natural fire curves

In a localized fire, there is an accumulation of smoke and hot gas in a layer below the ceiling (upper layer), with a horizontal interface between this layer and the cold lower layer when the gas temperature remains much lower. The thermal action of a

localized fire can be assessed using the method Heskestad. Localized fire temperature-time curve may be calculated according to:

$$\theta_z = 20 + 0{,}25 Q_c^{2/3} (z - z_0)^{-5/3} \tag{4}$$

Where $\theta_z$ is the temperature of the plume along the vertical flame axis [°C], $Q_c$ is the convective part of the heat release rate [W], $z$ is the height along the flame axis and z0 is the virtual origin of the fire, see Fig. 4.

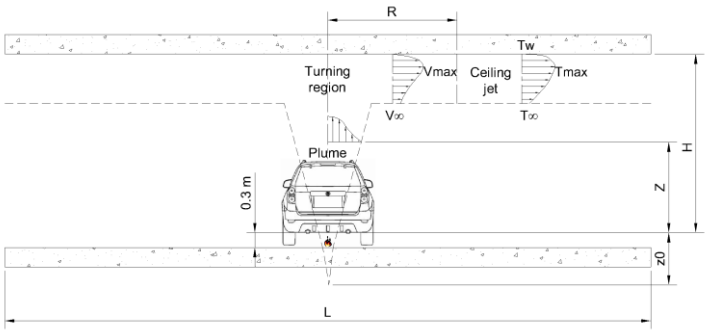


Fig. 4 - Parameters of localized fire.

The gas temperature representing the fire can also be given by the parametric temperature–time curve model given from annex A of EN 1991-1-2 [17]. This annex presents all equations required to calculate the temperature–time curve based on the value of the parameters that describe the particular situation. The model is valid for fire compartments up to 500 $m^2$ of floor area, maximum height of 4 meters without openings in the roof.

Parametric fires provide a simple means to take significant account physical phenomena that can influence the development of a fire in a particular building. As nominal fires, they provide a temperature-time curve, but these curves include some parameters intended to represent some real aspects in fire compartment. These curves have a heating and a cooling phase. The heating and cooling phase can be defined by the next equations.

$$\theta_g = 20 + 1325(1 - 0.324e^{-0,2t^*} - 0.204e^{-1,7t^*} - 0.472e^{-19t^*}) \tag{5}$$

$$\theta_g = \theta_{\max} - 250\left(t^* - t^*_{\max}\right) \tag{6}$$

Where $\theta_g$ is the gas temperature in the fire compartment [°C], t is the time [min]; $t^*$ is the time parameter that depends on the time factor, which itself depends on the opening factor and on the thermal absorptivity.

Fig. 5 represents the variation of temperature versus time for natural fire curves.

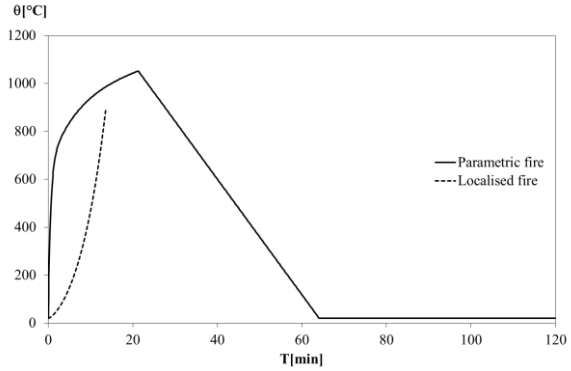


Fig. 5 - Natural fire curves.

EN 1991-1-2 [17] allows the utilisation of CFD (Computational Fluid Dynamics) models. Although EN 1991-1-2 [17] states under Clause 3.3.2 (2) that a method is given in Annex D for the calculation of thermal actions in case of CFD models, this annex simply gives general principles that form the base of the method and must be respected when establishing a software that allows application of this method in order to estimate the temperature field in the compartment. No guidance is provided on the manner to deduce the heat flux on the surface of the structural elements from the temperatures calculated in the compartment by the CFD model. In fact, this topic is still nowadays a subject of ongoing research activities and is probably premature to layout recommendations in a Code. The Eurocode allows the application of the CFD models in fire safety engineering but, this only can be made by well experienced user. Computational Fluid Dynamics (CFD) may be used to analyse fires in general, solving the Navier-Stokes equations, energy equation, and continuity equation, with special models for turbulence and radiation models. The equation for species can also be activated if the fire source is well established.

The next figures show a fire event with a class 1 car vehicle, burning in the centre of a fire compartment with the overall dimension of 10x10x3 $m^3$. This

compartment assumes the use of symmetry boundary conditions, allowing to model only one quarter of the full compartment. This compartment has two openings on the left side and right side, a concrete slab on the bottom and top floor and a concrete wall in the front and rear façade. The thermal load is defined by the Heat Released Rate. Three types of boundary conditions were applied (fixed wall with thermal conduction through thickness, pressure out let and symmetry). The solution method monitors the residuals for all variables and assumes the convergence of the solution for continuity (residual less than 0,01), velocity components (residual less than 0,001), energy (residual less than 0,00001), turbulence parameters (residual less than 0,001) and radiation parameters (residual less than 0,000001).

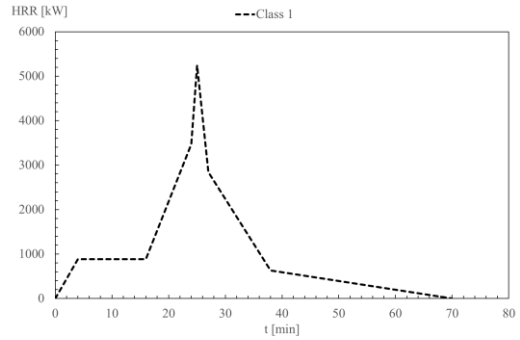


a) Heat release rate of a car class 1.

b) 3D model for fire simulation.

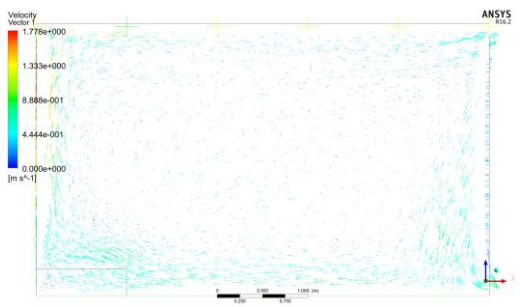


c) Velocity of the particles for 25 min.

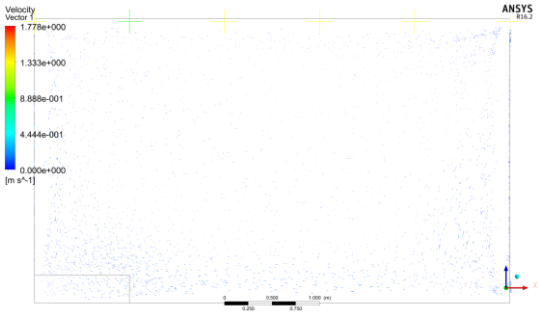


d) Velocity of the particles for 70 min.

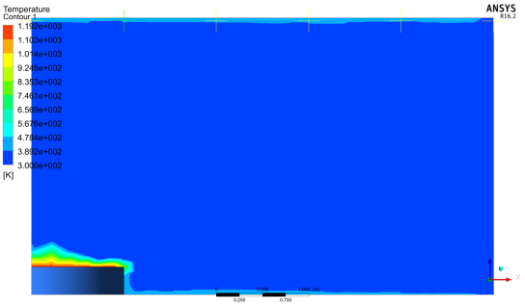


e) Temperature for 25 min.

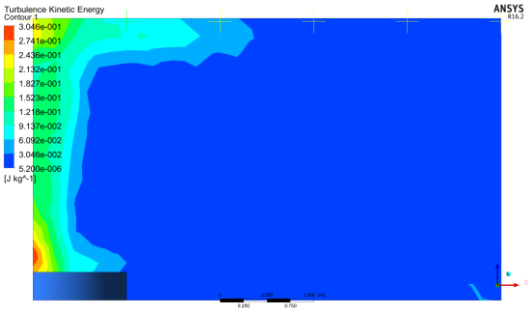


f) kinetics energy for 25 min.

Fig. 6 - Fire event with a class 1 car vehicle simulated by Fluent software.

### 2-2- Heat transfer

The modes of heat transfer are defined in Eurocode EN 1991-1-2 [17]. The net heat flux to unit surface area $\dot{h}_{net}\ \left[W/m^2\right]$ is going to be defined on the surface of the element. All surfaces exposed to fire must assume the transfer of heat by convection and radiation, given by the following expression.

$$\dot{h}_{net,d} = \dot{h}_{net,c} + \dot{h}_{net,r} \quad \left[W/m^2\right] \tag{7}$$

The convection heat transfer is the energy that is transferred between a solid and a moving fluid or gas, each being at different temperatures. The rate at which this exchange of energy occurs is given by Newton's law of cooling, shown Eq.(8).

$$\dot{h}_{net,c} = \alpha_c\left(\theta_g - \theta_m\right) \quad \left[W/m^2\right] \tag{8}$$

Where, $\alpha_c$ Is the heat transfer coefficient by convection $\left[W/m^2K\right]$, $\theta_g$ is the gas temperature in the vicinity of the fire exposed member $\left[^0C\right]$, and $\theta_m$ is the surface temperature of the member $\left[^0C\right]$.

The convection coefficient value depends on the velocity of the fluid or gas and should be considered equal to 9, 25 and 50 for cases of non-exposed surface, exposed surface with ISO834 curve [4] and exposed surface with hydrocarbons.

The heat transfer by radiation represents the energy transfer between two bodies through electromagnetic waves. This form of energy transfer is exhibit by all bodies, and requires no medium for the heat to be transferred. It can even occur in a vacuum the amount of energy that can be radiated by a surface is given by the Stefen-Boltzmann law shown in Eq.(9) .

$$\dot{h}_{net,r} = \phi \times \varepsilon_f \times \varepsilon_m \times \sigma\left[\left(\theta_r + 273\right)^4 - \left(\theta_m + 273\right)^4\right] \quad \left[W/m^2\right] \tag{9}$$

Where $\phi$ represents the view factor; $\varepsilon_f$ represents the emissivity of the fire; $\varepsilon_m$ is the emissivity of the surface of the element; $\sigma$ is the Stephan Boltzmann constant

$5{,}67 \times 10^{-8}$ $[W/m^2K^4]$; $\theta_r$ represents is the effective radiation temperature of the fire environment $[^0C]$; $\theta_m$ represents the surface temperature of the member $[^0C]$.

The emissivity of the material for steel and concrete is equal to $\varepsilon_m = 0{,}7$. The emissivity of the fire (flames) is assumed $\varepsilon_f = 1{,}0$ and the view factor can be assumed equal to 1,0 when not specified.

### 2-3- Materials properties

#### 2-3-1- Thermal properties

##### 2-3-1-1- Steel profile and reinforcing

The Specific heat of steel represents the amount of energy that is necessary to raise the unit mass of steel temperature by $1[°C]$, it is also the measure of the materials ability to absorb heat. The specific heat of steel $C_a$ defined in accordance to Eurocode EN1993-1-2 [18] as the following:

$20[°C] \le \theta < 600[°C]$:

$$C_a = 425 + 7{,}73.10^{-1}\theta_a - 1{,}69.10^{-3}\theta_a^2 + 2{,}22.10^{-6}\theta_a^3 \ [\text{J/kg.k}] \quad (10)$$

$600[°C] \le \theta < 735[°C]$:

$$C_a = 666 + \frac{13002}{(738 - \theta_a)} \ [\text{J/kg.k}] \quad (11)$$

$735[°C] \le \theta < 900[°C]$:

$$C_a = 545 + \frac{17820}{(\theta_a - 731)} \ [\text{J/kg.k}] \quad (12)$$

$900[°C] \le \theta \le 1200[°C]$:

$$C_a = 650 \ [\text{J/kg.k}] \quad (13)$$

Fig. 7 represents the variation of specific heat with temperature.

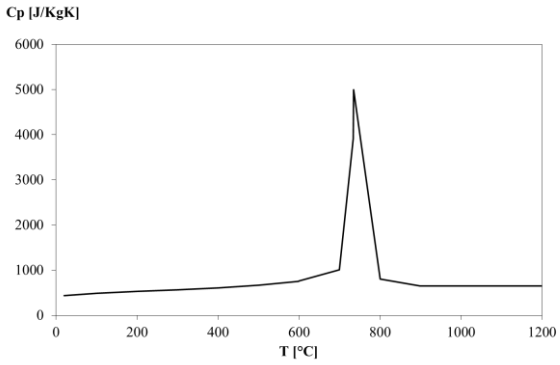


Fig. 7 - Specific heat at elevated temperature.

Thermal conductivity is the coefficient which dictates the rate which heat arriving at the steel surface is conducted through the metal. According to Eurocode EN1993-1-2 [18] the variation of thermal conductivity with temperature is represented in Fig. 8. The thermal conductivity of steel $\lambda_a$ should be determined from the following:

$20[°C] \le \theta < 800[°C]$:

$$\lambda_a = 54 - 3{,}33.10^{-2}\,\theta_a \ \left[\text{w/mk}\right] \tag{14}$$

$800[°C] \le \theta \le 1200[°C]$:

$$\lambda_a = 27{,}3 \ \left[\text{w/mk}\right] \tag{15}$$

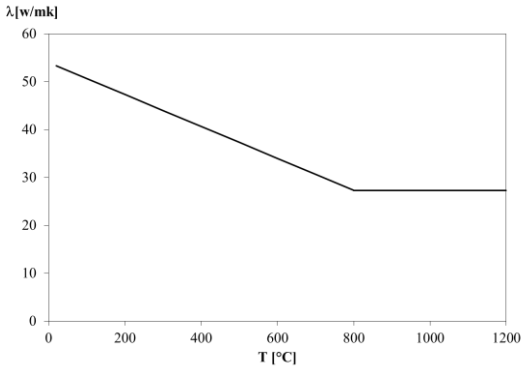


Fig. 8 - Thermal conductivity at elevated temperature

The density of steel is constant $\rho$=7850 kg/m$^3$, even when the temperature is modified. According to Eurocode EN1993-1-2 [18] the variation of thermal conductivity is represented in Fig. 9.

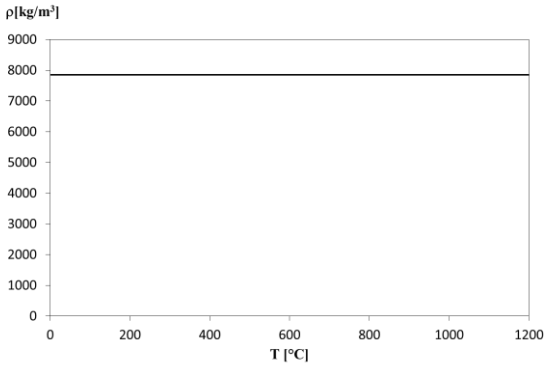


Fig. 9 - Density of steel at elevated temperature

### 2-3-1-2- Concrete

The specific heat of concrete varies mainly with the moisture content. The moisture within the concrete causes a peak between $100[°C]$ and $200[°C]$ due to the water being driven off. Fig. 10 depicts the variation of this property with temperature The pick value depends on the amount of moisture, in this case $u = 3\%$ was assumed, The Eurocode EN 1992-1-2 [19] recommends the following relationship for calculation of concrete specific heat.

$20[°C] \le \theta \le 100[°C]$:

$$C_P(\theta) = 900 \tag{16}$$

$100[°C] < \theta \le 115[°C]$:

$$C_P(\theta) = 2020 \tag{17}$$

$115[°C] < \theta \le 200[°C]$:

$$C_P(\theta) = 2020 - (\theta - 115)/12 \tag{18}$$

$200[°C] < \theta \le 400[°C]$:

$$C_P(\theta) = 1000 + (\theta - 200)/2 \tag{19}$$

$400[°C] < \theta \le 1200[°C]$:

$$C_P(\theta) = 1100 \tag{20}$$

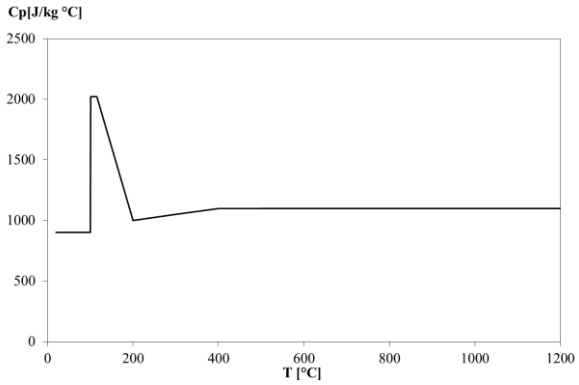


Fig. 10 - Specific heat at elevated temperature.

The thermal conductivity depends upon the aggregate type and the temperature of the concrete. The thermal conductivity $\lambda_c$ of concrete may be determined between lower and upper limit values. Fig. 11 represent the variation of the upper limit of thermal conductivity with temperature. The following equation defined in Eurocode EN 1992-1-2 [19] recommends the upper limit for normal weight concrete.

$$\lambda_c = 2 - 0.2451(\theta/100) + 0.0107(\theta/100)^2 \quad [\text{w/mk}] \tag{21}$$

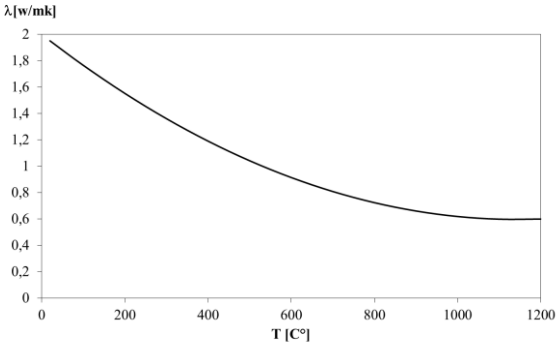


Fig. 11 - Thermal conductivity at elevated temperature.

Density is a physical property of matter. In a qualitative manner density is defined as the heaviness of objects with a specific volume. It is denoted as ρ. Common unit of density is kg/m$^3$. Fig. 12 represents the variation of density with temperature. We have ρ(20°C)=2300 Kg/m$^3$, The Eurocode EN 1992-1-2 [19] recommends the following relationship for calculation of concrete density.

$20[°C] \le \theta \le 115[°C]$:

$$\rho(\theta) = \rho(20°C) \tag{22}$$

$115[°C] < \theta \le 200[°C]$:

$$\rho(\theta) = \rho(20°C).(1 - 0{,}02(\theta - 115)/85) \tag{23}$$

$200[°C] < \theta \le 400[°C]$:

$$\rho(\theta) = \rho(20°C).(0{,}98 - 0{,}03(\theta - 200)/200) \tag{24}$$

$400[°C] < \theta \le 1200[°C]$:

$$\rho(\theta) = \rho(20°C).(0{,}95 - 0{,}07(\theta - 400)/800) \tag{25}$$

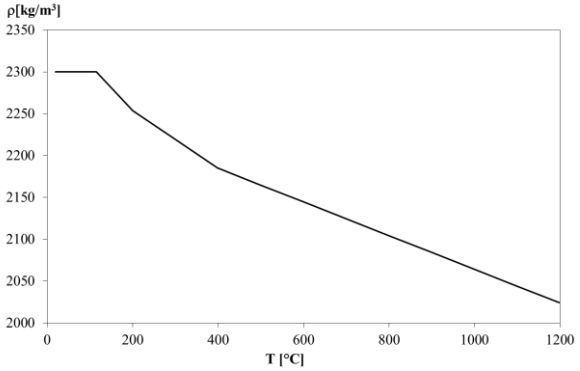


Fig. 12 - Density of concrete at elevated temperature.

### 2-3-2- Mechanical properties

#### 2-3-2-1- Steel profile S275

The nominal resistance of steel profiles is characterized in European standards Eurocode EN1993-1-1 [2] for room temperature and Eurocode EN1993-1-2 [18] for elevated temperatures (the action of fire). The values of the yield and ultimate stress, $f_y$ and $f_u$, are defined in this document. Under normal conditions the S275 steel, with thickness less than 40mm, presents the mechanical properties described in Table 3 and Fig. 13 shows the variation of the stress-strain relationship at different temperature levels.

To take into account the effect of high temperatures on the mechanical properties of the steel, reduction factors are proposed, according to EN 1993-1-2 [18].

The reduction factors for the proportional limit $k_{p,\theta}$, to the effective yield strength $k_{y,\theta}$ and to the slope of the linear elastic range $k_{E,\theta}$ are provided in Fig. 14. The stress-strain relationship for steel at elevated temperatures is represented in Table 4.

Table 3 - Mechanical characteristics of steel S275.

| $E_a\ [GPa]$ | $f_y\ [MPa]$ | $f_u\ [MPa]$ | $G_a\ [GPa]$ | $\nu$ |
|---|---|---|---|---|
| 210 | 275 | 430 | 81 | 0,3 |

Table 4 - Stress-strain relationship for steel at elevated temperatures.

| Strain range | Stress σ | Tangent modulus |
|---|---|---|
| $\varepsilon \le \varepsilon_{p,\theta}$ | $\varepsilon\, E_{a,\theta}$ | $E_{a,\theta}$ |
| $\varepsilon_{p,\theta} < \varepsilon < \varepsilon_{y,\theta}$ | $f_{p,\theta} - c + (b/a)\left[a^2 - (\varepsilon_{y,\theta} - \varepsilon)^2\right]^{0.5}$ | $\dfrac{b(\varepsilon_{y,\theta} - \varepsilon)}{a\left[a^2 - (\varepsilon_{y,\theta} - \varepsilon)^2\right]^{0.5}}$ |
| $\varepsilon_{y,\theta} \le \varepsilon \le \varepsilon_{t,\theta}$ | $f_{y,\theta}$ | 0 |
| $\varepsilon_{t,\theta} < \varepsilon < \varepsilon_{u,\theta}$ | $f_{y,\theta}\left[1 - (\varepsilon - \varepsilon_{t,\theta})/(\varepsilon_{u,\theta} - \varepsilon_{t,\theta})\right]$ | - |
| $\varepsilon = \varepsilon_{u,\theta}$ | 0,00 | - |
| Parameters | $\varepsilon_{p,\theta} = f_{p,\theta}/E_{a,\theta} \quad \varepsilon_{y,\theta} = 0{,}02 \quad \varepsilon_{t,\theta} = 0{,}15 \quad \varepsilon_{u,\theta} = 0{,}20$ | |
| Functions | $a^2 = (\varepsilon_{y,\theta} - \varepsilon_{p,\theta})(\varepsilon_{y,\theta} - \varepsilon_{p,\theta} + c/E_{a,\theta})$<br>$b^2 = c(\varepsilon_{y,\theta} - \varepsilon_{p,\theta})E_{a,\theta} + c^2$<br>$c = \dfrac{(f_{y,\theta} - f_{p,\theta})^2}{(\varepsilon_{y,\theta} - \varepsilon_{p,\theta})E_{a,\theta} - 2(f_{y,\theta} - f_{p,\theta})}$ | |

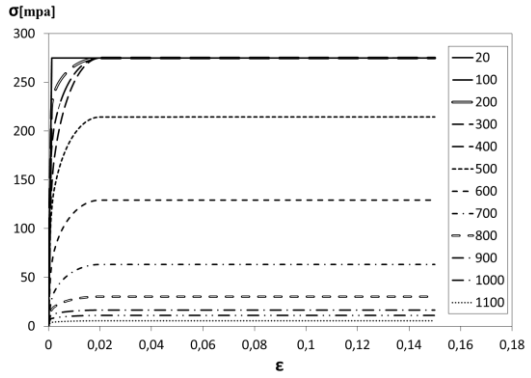


Fig. 13 - Curve stress-strain of steel under tention.

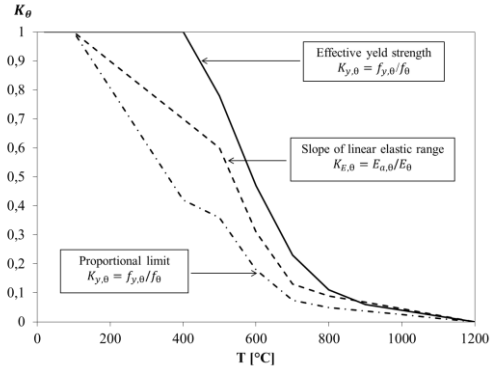


Fig. 14 - Reduction factors for the stress-strain relationship of steel at elevated temperatures.

### 2-3-2-2- Concrete C20 / 25

The concrete strength at room temperature is defined in Eurocode EN 1992-1-1 [20]. Eurocode EN1992-1-2 [19] is the reference document for this material under fire conditions. The material properties of concrete C20 / 25 at room temperature are shown in Table 5 the stress-strain relationship for concrete at elevated temperatures is illustrated in Table 6 and Fig. 15 showing the expected nonlinear variation.

The reduction of the characteristic compressive strength of concrete with the variation of the temperature T is allowed by the coefficient $k_{c,t(\theta)}$, this coefficient is represented in Fig. 16.

Table 5 - Mechanical characteristics of the concrete C20 / 25

| $f_{ck}\,[MPa]$ | $f_{ck,cube}\,[MPa]$ | $f_{cm}\,[MPa]$ | $f_{ctm}\,[MPa]$ | $E_{cm}\,[GPa]$ | $\varepsilon_{c1}\,[‰]$ | $\varepsilon_{cu1}\,[‰]$ |
|---|---|---|---|---|---|---|
| 20 | 25 | 28 | 2,2 | 30 | 2,0 | 3,5 |

Table 6 represents Stress-strain relationship for concrete at elevated temperatures.

Table 6 - Stress-strain relationship for concrete at elevated temperatures.

| Range | Stress σ(θ) |
|---|---|
| $\varepsilon \le \varepsilon_{c1,\theta}$ | $\dfrac{3.\varepsilon.f_{c\theta}}{\varepsilon_{c1,\theta}\left(2+\left(\dfrac{\varepsilon}{\varepsilon_{c1,\theta}}\right)^3\right)}$ |
| $\varepsilon_{c1,\theta} < \varepsilon \le \varepsilon_{cu1,\theta}$ | For numerical purposes a descending branch should be adopted. Linear or non linear models are permitted. |

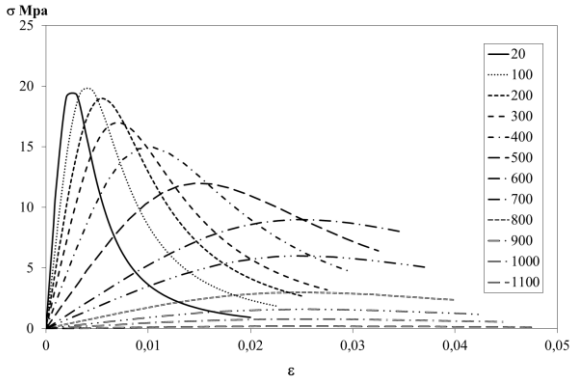


Fig. 15 - Curve stress-strain of concrete under compression.

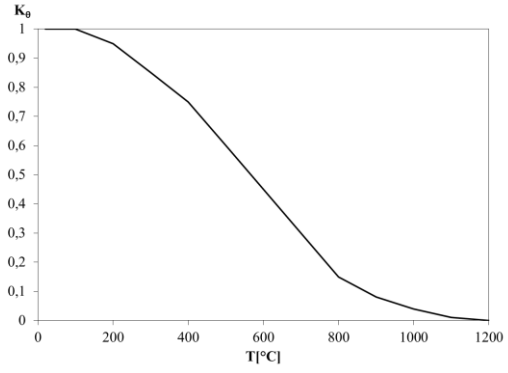


Fig. 16 - Reduction factors for the stress-train Relationship of concrete at elevated temperatures.

### 2-4-2-3- Reinforcing steel S500

The characteristics of the steel reinforcement is described in Eurocode EN 1992-1-1 [20]. Steel S500 NR, class B has the properties described in Table 7.

When subjected to high temperatures, Eurocode EN 1992-1-2 [19] defines reduction factors to be applied to the mechanical properties. The value of the yield stress $f_{sy,\theta}$, the value of proportional limit $f_{sp,\theta}$ and the value of the modulus of elasticity $E_{s,\theta}$ varies with temperature as can be seen in Fig. 18 the factors are represented to reduce the effective yield strength, and the modulus of elasticity. The stress-strain relationship for reinforcement at elevated temperatures is defined by Table 8, and Fig. 17 represents the curve variation of stress-strain.

Table 7 - Mechanical characteristics of steel S500.

| $E_s\ [GPa]$ | $f_{yk}\ [MPa]$ | $f_{uk}\ [MPa]$ | $G\ [GPa]$ | $k$ | $\nu$ |
|---|---|---|---|---|---|
| 210 | 500 | 540 | 81 | 1,08 | 0,3 |

Table 8 - Stress-strain relationship for reinforcement at elevated temperatures.

| Strain range $\varepsilon_{sp,\theta}$ | Stress σ $\varepsilon E_{s,\theta}$ | Tangent modulus $E_{s,\theta}$ |
|---|---|---|
| $\varepsilon_{sp,\theta} < \varepsilon < \varepsilon_{sy,\theta}$ | $f_{sp,\theta} - c + (b/a)\left[a^2 - (\varepsilon_{sy,\theta} - \varepsilon)^2\right]^{0.5}$ | $\frac{b(\varepsilon_{sy,\theta} - \varepsilon)}{a\left[a^2 - (\varepsilon - \varepsilon_{sy,\theta})^2\right]^{0.5}}$ |
| $\varepsilon_{sy,\theta} \le \varepsilon \le \varepsilon_{st,\theta}$ | $f_{sy,\theta}$ | 0 |
| $\varepsilon_{st,\theta} < \varepsilon < \varepsilon_{su,\theta}$ | $f_{sy,\theta}\left[1 - (\varepsilon - \varepsilon_{st,\theta})/(\varepsilon_{su,\theta} - \varepsilon_{st,\theta})\right]$ | - |
| $\varepsilon = \varepsilon_{su,\theta}$ | 0,00 | - |
| Parameters | $\varepsilon_{sp,\theta} = f_{sp,\theta}/E_{s,\theta}$ $\varepsilon_{sy,\theta} = 0{,}02$ $\varepsilon_{st,\theta} = 0{,}15$ $\varepsilon_{su,\theta} = 0{,}20$ | |
| Functions | $a^2 = (\varepsilon_{sy,\theta} - \varepsilon_{sp,\theta})(\varepsilon_{sy,\theta} - \varepsilon_{sp,\theta} + c/E_{s,\theta})$ | |
| | $b^2 = c(\varepsilon_{sy,\theta} - \varepsilon_{sp,\theta})E_{s,\theta} + c^2$ | |
| | $c = \frac{(f_{sy,\theta} - f_{sp,\theta})^2}{(\varepsilon_{sy,\theta} - \varepsilon_{sp,\theta})E_{s,\theta} - 2(f_{sy,\theta} - f_{sp,\theta})}$ | |

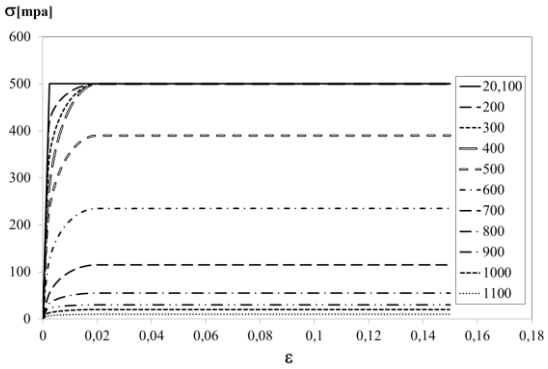


Fig. 17 - Curve stress-strain of reinforcement under tension.

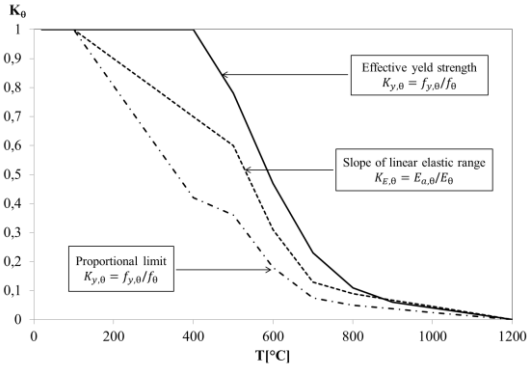


Fig. 18 - Reduction factors for the stress-strain relationship of rebars at elevated temperatures.

This page was intentionally left in blank

# CHAPTER.3 SIMPLIFIED METHOD USING EUROCODE 4-ANNEX G

Eurocode 4 part 1-2 [1] proposes different methods to determine the fire resistance of Partially Encased Columns under standard fire ISO834 [4]. The tabulated method uses values defined for the most common cross-sections based on experimental and empirical results. These results are generally very conservative and may be used for a preliminary design stage [21].

The simplified calculation method was originally developed Jungbluth [22] and was defined to determine the capacity of the PEC by dividing the section into four components. The current approach of this method is defined in Eurocode 4 part 1.2 [1] and is based on simple formulas and empirical coefficients that seem to be unsafe [23]. For this purpose, a new simple formulae was presented and is being validated [24].

The stability of PEC requires the calculation of the critical load and the effective flexural stiffness. These quantities depend on the temperature effect on the elastic modulus and on the second order moment of area of each component, according to Eq.(26).

$$\left(EI\right)_{fi,eff,z} = \varphi_{f,\theta}\left(EI\right)_{fi,f,z} + \varphi_{w,\theta}\left(EI\right)_{fi,w,z} + \varphi_{c,\theta}\left(EI\right)_{fi,c,z} + \varphi_{s,\theta}\left(EI\right)_{fi,s,z} \qquad (26)$$

In this equation $(EI)_{fi,eff,z}$ represents the effective flexural stiffness of the composite section in fire, $(EI)_{fi,f,z}$ represents effective flexural stiffness of the flange, $(EI)_{fi,w,z}$ represents effective flexural stiffness of the web, $(EI)_{fi,c,z}$ represents the effective flexural stiffness of the concrete and $(EI)_{fi,s,z}$ represents the effective flexural stiffness of reinforcement. The contribution of each part is going to be weighted according to $\varphi$ factors, a reduced modulus of elasticity and a reduced cross-section. These values depend on the fire rating, according to Table 9.

Table 9 - Reduction coefficients for bending stiffness around the week axis.

| Standard fire resistance class | $\varphi_{f,\theta}$ | $\varphi_{w,\theta}$ | $\varphi_{c,\theta}$ | $\varphi_{s,\theta}$ |
|---|---|---|---|---|
| R30 | 1,0 | 1,0 | 0,8 | 1,0 |
| R60 | 0,9 | 1,0 | 0,8 | 0,9 |
| R90 | 0,8 | 1,0 | 0,8 | 0,8 |
| R120 | 1,0 | 1,0 | 0,8 | 1,0 |

The elastic buckling load $N_{fi,cr,z}$ requires the calculation of the effective flexural stiffness of the composite section in fire $(EI)_{fi,eff,z}$. The non-dimensional slenderness ratio $\bar{\lambda}_\theta$ and $N_{fi,cr,z}$ are calculated according to Eqs.(27 -(29), when the safety partial factors are assumed equal to 1.0. The buckling length of the column under fire conditions is represented by $L_\theta$. The calculation of the axial plastic resistance under fire $N_{fi,pl,Rd}$ the cross-section is divided into four components according to Eq.(27).

$$N_{fi,pl,Rd} = N_{fi,pl,Rd,f} + N_{fi,pl,Rd,w} + N_{fi,pl,Rd,c} + N_{fi,pl,Rd,s} \quad (27)$$

$$\bar{\lambda}_\theta = \sqrt{N_{fi,pl,Rd} / N_{fi,cr,z}} \quad (28)$$

$$N_{fi,cr,z} = \pi^2 / L_\theta^2 \times (EI)_{fi,eff,z} \quad (29)$$

This calculation method takes into consideration the effect of the fire in four components of the cross section. The four components are identified in Fig. 19 and include: the flange component, the web component, the concrete and reinforcement components.

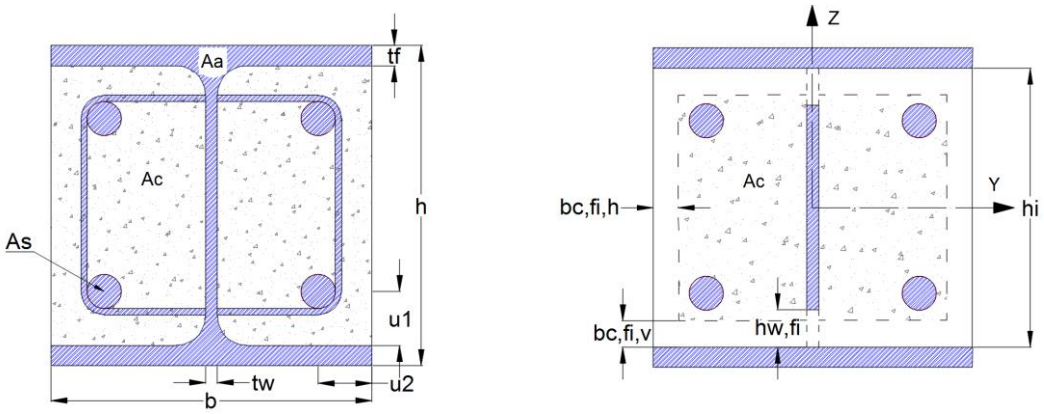


Fig. 19- Reduced cross-section for structural fire design.

### 3-1- Definition of partially encased column

Partially Encased Columns (PEC) have excellent axial buckling resistance under fire. The PEC are usually made of hot rolled steel profiles, reinforced with concrete between the flanges. Due to the thermal and mechanical properties of concrete, composite columns always presents higher fire resistance than steel bare columns. The composite section is responsible for increasing the torsional and bending stiffness when

compared to the same section of the steel profile, the formwork and the connection with the beam is easily when compared with the solution of totally encased column. In addition to these advantages, the reinforced concrete is responsible for increasing the fire resistance.

Fig. 20 - Example of partially encased column.

Twenty-four different cross sections were selected to analyse the effect of fire: ten steel IPE profiles ranging from 200 to 500 and fourteen steel HEB ranging from 160 to 500. These columns were tested under standard fire ISO834 [4], using three buckling length explained in Fig. 21 , using 3m and 5m column height. S275 and B500 grades were selected to steel while C20/25 grade was considered to concrete.

The cross sections were defined accordingly to the tabular design method for Partially Encased Columns under fire [1]. This leads to minimum dimensions and minimum distances between components. The design of this section depends on the load level, and on the ratio between the thickness of the web and the thickness of the flange see Table 10. This tabular method applies to structural steel grades S235, S275 and S355 and to a minimum value of reinforcement, between 1 and 6%.

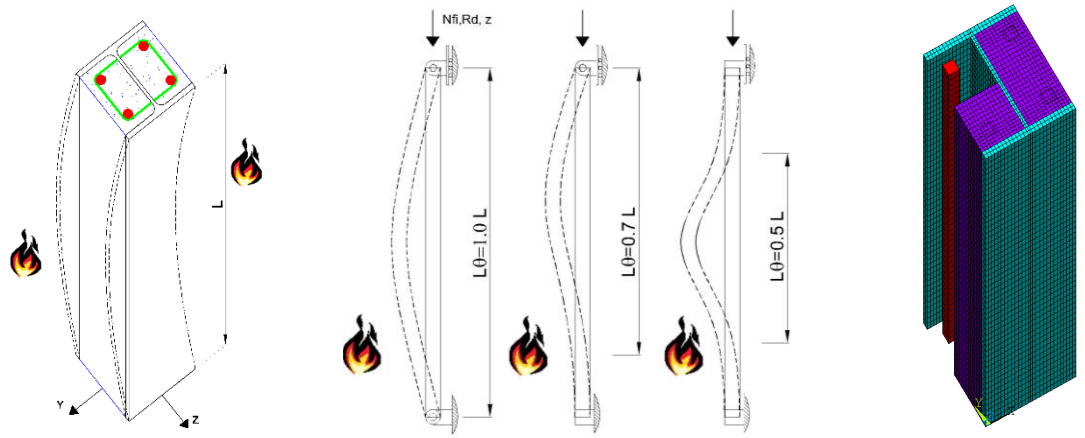


a) Buckling deformed shape b) Buckling length in fire c) Finite element approximation

Fig. 21 - Partially encased column under fire.

Table 10 presents the main dimensions of the cross section, in particular the number of rebars, the diameter of each rebar, the cover dimensions in both principal directions.

Table 10 - Characteristics of the sections under study.

| profile | Nº of rebars | $\Phi$ $[mm]$ | $A_s$ $[mm^2]$ | $A_c$ $[mm^2]$ | $u_1$ $[mm]$ | $u_2$ $[mm]$ | $u$ $[mm]$ | $\frac{A_s}{A_s + A_c}$ | $\frac{t_w}{t_f}$ | $A_m/V$ $[mm^{-1}]$ |
|---|---|---|---|---|---|---|---|---|---|---|
| HEB160 | 4 | 12 | 452 | 19916 | 40 | 40 | 40 | 2,22 | 0,62 | 3,61 |
| HEB180 | 4 | 12 | 452 | 25616 | 40 | 40 | 40 | 1,74 | 0,61 | 2,86 |
| HEB200 | 4 | 20 | 1257 | 31213 | 50 | 50 | 50 | 3,87 | 0,60 | 6,45 |
| HEB220 | 4 | 25 | 1963 | 37611 | 50 | 50 | 50 | 4,96 | 0,59 | 8,36 |
| HEB240 | 4 | 25 | 1963 | 45417 | 50 | 50 | 50 | 4,14 | 0,59 | 7,05 |
| HEB260 | 4 | 32 | 3217 | 53033 | 50 | 50 | 50 | 5,72 | 0,57 | 10,01 |
| HEB280 | 4 | 32 | 3217 | 62541 | 50 | 50 | 50 | 4,89 | 0,58 | 8,39 |
| HEB300 | 4 | 32 | 3217 | 72501 | 50 | 50 | 50 | 4,25 | 0,58 | 7,34 |
| HEB320 | 4 | 32 | 3217 | 77275 | 50 | 50 | 50 | 4,00 | 0,56 | 7,12 |
| HEB340 | 4 | 40 | 5027 | 80509 | 50 | 50 | 50 | 5,88 | 0,56 | 10,53 |
| HEB360 | 4 | 40 | 5027 | 85536 | 50 | 50 | 50 | 5,55 | 0,56 | 9,99 |
| HEB400 | 4 | 40 | 5027 | 95821 | 70 | 50 | 59 | 4,98 | 0,56 | 8,86 |
| HEB450 | 4 | 40 | 5027 | 108801 | 70 | 50 | 59 | 4,42 | 0,54 | 8,20 |
| HEB500 | 4 | 40 | 5027 | 121735 | 70 | 50 | 59 | 3,97 | 0,52 | 7,66 |
| IPE200 | 4 | 12 | 452 | 16823 | 50 | 40 | 45 | 2,62 | 0,66 | 3,97 |
| IPE220 | 4 | 20 | 1257 | 19730 | 50 | 40 | 45 | 5,99 | 0,64 | 9,34 |
| IPE240 | 4 | 20 | 1257 | 23825 | 50 | 40 | 45 | 5,01 | 0,63 | 7,92 |
| IPE270 | 4 | 25 | 1963 | 30085 | 50 | 40 | 45 | 6,13 | 0,65 | 9,47 |
| IPE300 | 4 | 25 | 1963 | 37848 | 50 | 40 | 45 | 4,93 | 0,66 | 7,43 |
| IPE330 | 4 | 25 | 1963 | 44854 | 50 | 40 | 45 | 4,19 | 0,65 | 6,43 |
| IPE360 | 4 | 32 | 3217 | 50988 | 50 | 40 | 45 | 5,93 | 0,63 | 9,42 |
| IPE400 | 4 | 32 | 3217 | 60715 | 70 | 40 | 53 | 5,03 | 0,64 | 7,90 |
| IPE450 | 4 | 32 | 3217 | 72779 | 70 | 40 | 53 | 4,23 | 0,64 | 6,57 |
| IPE500 | 4 | 40 | 5027 | 83800 | 70 | 50 | 59 | 5,66 | 0,64 | 8,88 |

### 3-2- Flanges of the steel profile

The average flange temperature $\theta_{f,t}$ must be determined according to the next formula. The value depends on the empirical coefficient $k_t$ , on the reference value $\theta_{0,t}$ and on the section factor $A_m/V$ :

$$\theta_{f,t} = \theta_{0,t} + k_t\left(A_m/V\right) \tag{30}$$

The empirical coefficient shown in this table:

Table 11 - Parameters for the flange temperature

| Standard Fire Resistance | $\theta_{0,t}$ $[m^{o}C]$ | $k_t$ $[m^{o}C]$ |
|---|---|---|
| R30 | 550 | 9,65 |
| R60 | 680 | 9,55 |
| R90 | 805 | 6,15 |
| R120 | 900 | 4,65 |

The average temperature of the flange allows the calculation of the fire effect on the mechanical properties. This effect is defined by the reduction coefficients, $K_{y,\theta}$ and $K_{E,\theta}$, used for the Modulus of elasticity and to the yield stress, being determined from:

$$f_{ay,f,t} = f_{ay,f}K_{y,\theta} \tag{31}$$

$$E_{ay,f,t} = E_{ay,f}K_{E,\theta} \tag{32}$$

The plastic resistance to axial compression and the flexural stiffness of the two flanges of the steel profile in the fire situation are determined from:

$$N_{fi,pl,rd,f} = 2\left(b_{ef}\, f_{ay,f,t}\right)/\,\delta_{M,fe,a} \tag{33}$$

$$\left(EI\right)_{fi,f,z} = E_{a,f,t}\left(e_f b^3\right)/6 \tag{34}$$

### 3-3- Web of the steel profile

The part of the web to be neglected is defined by $h_{w,fi}$ . The fire effect is responsible to decrease the height of the resistant web, starting at the inner edge of the flange (see Fig. 19). This part is determined from:

$$h_{w,fi} = 0{,}5\left(h - 2e_f\right)\left(1 - \sqrt{1 - 0.16\left(H_t / h\right)}\right) \tag{35}$$

The parameter $H_t$ it's given according to the table:

Table 12 - Parameter for height reduction of the web

| Standard Fire Resistance | $H_t[mm]$ |
|---|---|
| R30 | 350 |
| R60 | 770 |
| R90 | 1100 |
| R120 | 1250 |

The yield stress is modified from:

$$f_{ay,w,t} = f_{ay,w,t}\sqrt{1 - 0.16\left(H_t / h\right)} \tag{36}$$

The design value of the plastic resistance to axial compression and the flexural stiffness of the web of the steel profile in the fire situation are determined from:

$$N_{fi,pl,rd,w} = \left[ew\left(h - 2e_f - 2h_{w,fi}\right)\right]f_{ay,w,t} / \delta_{M,fi,a} \tag{37}$$

$$\left(EI\right)_{fi,w,t} = \left[E_{a,w}\left(h - 2e_f - 2h_{w,fi}\right)\right]e_w^3 / 12 \tag{38}$$

### 3-4- Partially Encased Concrete

An exterior layer of concrete with a thickness $b_{c,fi}$ is going to be neglected in the calculation (see Fig. 19). The thickness $b_{c,fi}$ is given in Table 13, and depends on the section factor $A_m/V$ , of the entire composite cross-section, only for fire ratings of 90 minutes and 120 minutes.

Table 13 - Thickness reduction of the concrete area.

| Standard Fire Resistance | $b_{c,\,fi}\ [mm]$ |
|---|---|
| R30 | 4.0 |
| R60 | 15.0 |
| R90 | $0.5(\mathrm{A_m}/V) + 22.5$ |
| R120 | $2.0(\mathrm{A_m}/V) + 24.0$ |

The average temperature in concrete $\theta_{c,t}$ is given in Table 14 and depends on the section factor $A_m/V$ of the entire composite cross-section and on the fire rating class.

Table 14 - Average concrete temperature.

| R30 | | R60 | | R90 | | R120 | |
|---|---|---|---|---|---|---|---|
| $A_m/V\left[m^{-1}\right]$ | $\theta_{c,t}\left[^{o}C\right]$ | $A_m/V\left[m^{-1}\right]$ | $\theta_{c,t}\left[^{o}C\right]$ | $A_m/V\left[m^{-1}\right]$ | $\theta_{c,t}\left[^{o}C\right]$ | $A_m/V\left[m^{-1}\right]$ | $\theta_{c,t}\left[^{o}C\right]$ |
| 4 | 136 | 4 | 214 | 4 | 256 | 4 | 265 |
| 23 | 300 | 9 | 300 | 6 | 300 | 5 | 300 |
| 46 | 400 | 21 | 400 | 13 | 400 | 9 | 400 |
| | | 50 | 600 | 33 | 600 | 23 | 600 |
| | | | | 54 | 800 | 38 | 800 |
| | | | | | | 41 | 900 |
| | | | | | | 43 | 1000 |

The secant modulus of concrete at elevated temperature is obtained from the next expression and is going to affect the effective flexural stiffness:

$$E_{c,\mathrm{sec},\theta} = f_{c,\theta} / \varepsilon_{cu,\theta} = f_c K_{c,\theta} / \varepsilon_{cu,\theta} \tag{39}$$

The design value of the plastic resistance to axial compression considers the effect of the material temperature and the residual cross section. The effective flexural stiffness of the concrete in the fire considers the residual area of concrete, being both parameters are determined from:

$$N_{fi,pl,Rd,c} = 0{,}86\left[\left(\left(h - 2e_f - 2b_{c,\,fi}\right)\left(b - e_w - 2b_{c,\,fi}\right)\right) - A_s\right] f_{c,\theta} / \delta_{M,\,fi,c} \tag{40}$$

Where $A_s$ is the cross-section of the reinforcing bars.

$$\left(EI\right)_{fi,c,z} = E_{c,\mathrm{sec},\theta}\left[\left\{\left(h - 2e_f - 2b_{c,\,fi}\right)\left(\left(b - 2b_{c,\,fi}\right)^3 - e_w^3\right)/12\right\} - I_{s,z}\right] \tag{41}$$

Where $I_{s,z}$, is the second moment of area of the reinforcing bars related to the central axis Z of the composite cross-section.

### 3-5- Reinforcing bars

The reduction factor $k_{y,t}$ of the yield stress and the reduction factor $k_{E,t}$ of the modulus of elasticity of the reinforcing bars depend on the fire rating and on the position of the reinforcement, being the geometrical average u representative of the distances of the reinforcement to the outer borders of the concrete (see

Table 15 and Table 16).

Table 15 - Reduction factor $k_{y,t}$ for the yield point $f_{s,y}$ of the reinforcing bars.

| | Standard Fire Resistance | | | |
|---|---|---|---|---|
| u [mm] | R30 | R60 | R90 | R120 |
| 40 | 1 | 0,789 | 0,314 | 0,17 |
| 45 | 1 | 0,883 | 0,434 | 0,223 |
| 50 | 1 | 0,976 | 0,572 | 0,288 |
| 55 | 1 | 1 | 0,696 | 0,367 |
| 60 | 1 | 1 | 0,822 | 0,436 |

Table 16 - Reduction factor $k_{E,t}$ for the modulus of elasticity of the reinforcing bars.

| | Standard Fire Resistance | | | |
|---|---|---|---|---|
| u [mm] | R30 | R60 | R90 | R120 |
| 40 | 0,83 | 0,604 | 0,193 | 0,11 |
| 45 | 0,865 | 0,647 | 0,283 | 0,128 |
| 50 | 0,888 | 0,689 | 0,406 | 0,173 |
| 55 | 0,914 | 0,729 | 0,522 | 0,233 |
| 60 | 0,935 | 0,763 | 0,619 | 0,285 |

The geometrical average u of the axis distances $u_1$ and $u_2$ is obtained from $u = \sqrt{u_1.u_2}$, being $u_1$ the distance from the outer reinforcing bar to the inner flange edge in [mm] and $u_2$ is the distance from the outer reinforcing bar to the concrete surface [mm]. There are a few restraints to the calculation of the geometrical average u, see next equations.

$$(u_1 - u_2) > 10mm, \qquad then \qquad u = \sqrt{u_2(u_2 + 10)} \tag{42}$$

$$(u_2 - u_1) > 10mm, \qquad then \qquad u = \sqrt{u_1(u_1 + 10)} \tag{43}$$

The design value of the plastic resistance to axial compression and the flexural stiffness of the reinforcing bars takes into account the effect of the temperature into the mechanical properties in the fire condition and are obtained from:

$$N_{fi,pl,Rd,s} = A_s k_{y,t} f_{s,y} / \delta_{M,fi,s} \tag{44}$$

$$(EI)_{fi,s,z} = k_{E,t} E_s I_{s,z} \tag{45}$$

The partial safety factor can be considered equal to 1.

This page was intentionally left in blank

# CHAPTER.4 NEW PROPOSAL FORMULAE FOR ANNEX G

## 4-1- Introduction

The new proposal is to be applied to the balanced summation model and is considered a simple calculation method. All the intermediate calculations are presented in Annex . Fig. 22 present the Isothermal criteria used for new proposal.

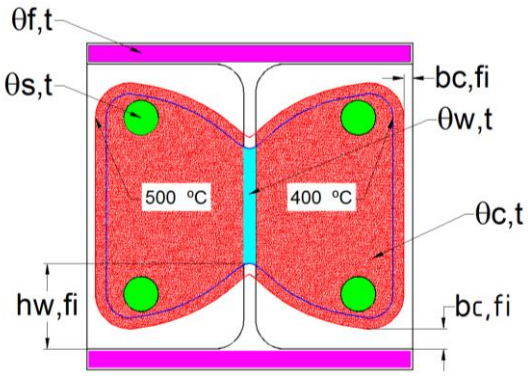


Fig. 22 - Isothermal criteria in the cross section.

## 4-2- Fire effect on the flange component

The effect of fire in the flange component requires a bilinear approximation for the calculation of the average temperature in flange, using a new empirical coefficient $k_t$ and a new reference value $\theta_{0,t}$ , see Eq.(46) and Table 17.

Fig. 23 represents the average temperature of the flange, depending on the section factor and on the standard fire resistance class. Each graph depicts the results of the simplified calculation method based on the current version of the Eurocode, the results of the advanced calculation method based on a 2D analysis (ANSYS) and the results of the new formulae by approximation to the numerical simulation results.

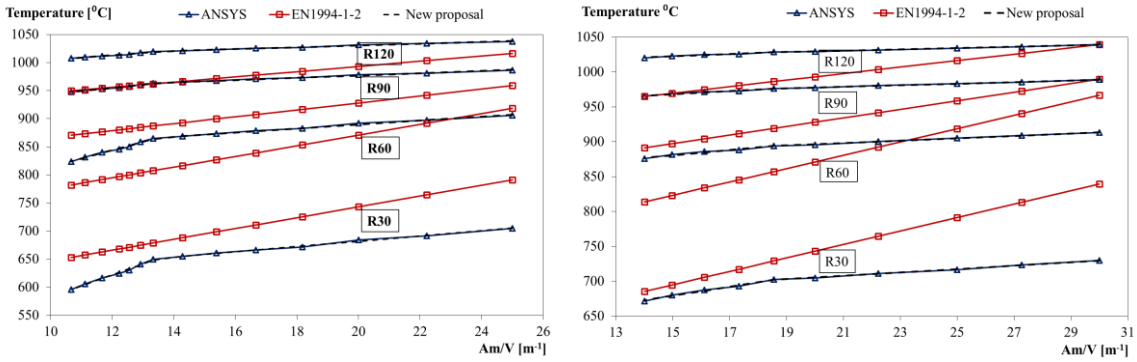


a) HEB sections b) IPE section

Fig. 23 - Average temperature of the flange.

The temperature is affecting the elastic modulus of the material without any other reduction that could affect the second order moment of area.

$$\theta_{f,t} = \theta_{0,t} + k_t\left(A_m/V\right) \tag{46}$$

The new proposal presents a new value for the reference temperature and a new value for the empirical coefficient.

Table 17 - Parameters for determining the temperature in the flange.

| Sections | 10<Am/V<14 | | 14<=Am/V<25 | | 10<Am/V<19 | | 19<=Am/V<30 | |
|---|---|---|---|---|---|---|---|---|
| | HEB | | HEB | | IPE | | IPE | |
| Standard Fire | $\theta_{0,t}$ [$^0$C] | $k_t$ [m$^0$C] | $\theta_{0,t}$ [$^0$C] | $k_t$ [m$^0$C] | $\theta_{0,t}$ [$^0$C] | $k_t$ [m$^0$C] | $\theta_{0,t}$ [$^0$C] | $k_t$ [m$^0$C] |
| R30 | 387 | 19,55 | 588 | 4,69 | 582 | 6,45 | 656 | 2,45 |
| R60 | 665 | 14,93 | 819 | 3,54 | 824 | 3,75 | 862 | 1,72 |
| R90 | 887 | 5,67 | 936 | 2,04 | 935 | 2,20 | 956 | 1,09 |
| R120 | 961 | 4,29 | 998 | 1,62 | 997 | 1,68 | 1010 | 0,96 |

### 4-3- Fire effect on the web component

The effect of the fire on the web of the steel section is determined by the 400 °C isothermal criterion [25-27]. This procedure defines the affected zone of the web and predicts the web height reduction $h_{w,fi}$, see

Fig. 24. This new formulae presents a strong dependence on the section factor $A_m/V$, regardless of the fire resistance class (t in minutes), unlike the current version of the Eurocode EN1994-1-2 [1].

The results of the current version of Eurocode EN1994-1-2 [1] are unsafe for all fire resistance classes and for all section factors. The new proposal presents a parametric expression that depends on section factor and on the standard fire resistance class, Eqs.(47)-(48). Both equations have the application limits defined in Table 18. This calculation is affecting the second order moment of area of the web, without considering any temperature effect on the reduction of the elastic modulus.

$$2h_{w,fi}/h_i \times 100 = 0.0035 \times t^2 \times (A_m/V) - 0.03 \times t^{2.02} + (A_m/V)/2 \ \text{for (HEB)} \quad (47)$$

$$2h_{w,fi}/h_i \times 100 = 0.002 \times t^2 \times (A_m/V) - 0.03 \times t^{1.933} + (A_m/V) \ \text{for (IPE)} \quad (48)$$

Table 18 - Application limits (HEB and IPE profiles).

| Standard fire resistance | Section factor (HEB) | Section factor (IPE) |
|---|---|---|
| R30 | $A_m/V$ <22,22 | $A_m/V$ <30 |
| R60 | $A_m/V$ <15,38 | $A_m/V$ <18,56 |
| R90 | $A_m/V$ <12,22 | $A_m/V$ <14,97 |
| R120 | $A_m/V$ <11,11 | - |

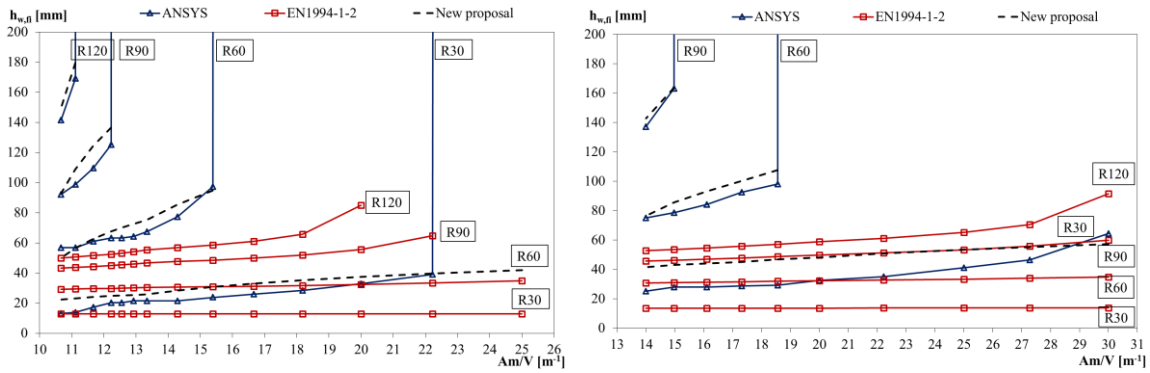


a) HEB sections b) IPE section

Fig. 24 - Web height reduction.

The arithmetic average temperature of the effective web section is depicted in Fig. 25 and was defined by the nodal position under the limiting condition, see Eq.(49) and Table 19. Temperature results of EN1994-1-2 [1] presented on this graph were determined by the inverse method, using the reduction factor of the yielding stress. The new proposal was adjusted to numerical results and a big difference between the current version and the new proposal is evident.

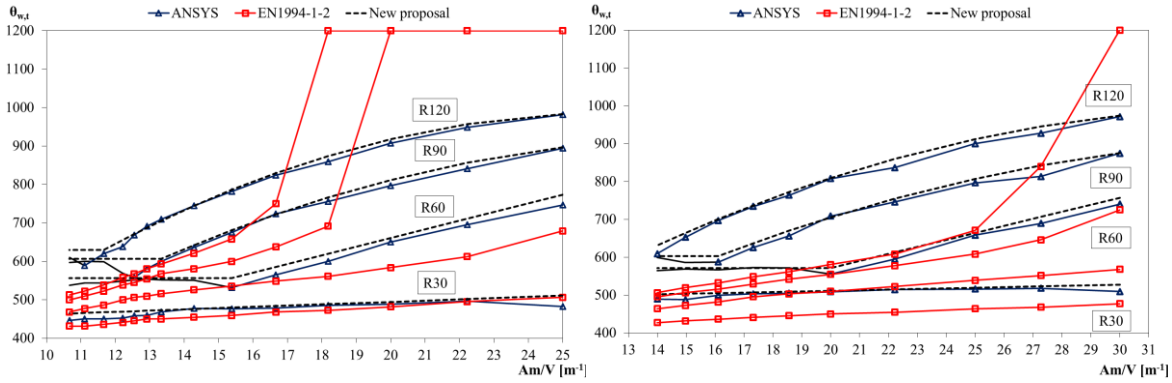


a) HEB sections b) IPE section

Fig. 25 - Average web temperature for different standard fire resistance classes.

$$\theta_{w,t} = a \times \left(A_m/V\right) \times 2 + b \times A_m/V + c \tag{49}$$

Table 19 - Parameters and application limits for HEB and IPE cross sections.

| Standard fire resistance | a (HEB) | b (HEB) | c (HEB) | Section factor (HEB) |
|---|---|---|---|---|
| R30 | 0.0000 | 3.2285 | 430.0000 | 10<Am/V<25 |
| R60 | 0.0000 | 0.0000 | 566.6500 | 10<Am/V<15 |
| | 0.0000 | 22.5320 | 210.0000 | 15<Am/V<25 |
| R90 | 0.0000 | 0.0000 | 606.4000 | 10<Am/V<13 |
| | 1.1823 | 70.2440 | 120.0000 | 13<Am/V<25 |
| R120 | 0.0000 | 0.0000 | 629.8661 | 10<Am/V<11 |
| | -1.6136 | 85.6710 | -150.0000 | 11<Am/V<25 |

| Standard fire resistance | a (IPE) | b (IPE) | c (IPE) | Section factor (IPE) |
|---|---|---|---|---|
| R30 | 0.0000 | 1.5708 | 480.0000 | 14<Am/V<30 |
| R60 | 0.0000 | 0.0000 | 571.5400 | 14<Am/V<20 |
| | 0.0000 | 18.5770 | 200.0000 | 20<Am/V<30 |
| R90 | 0.0000 | 0.0000 | 602.8100 | 14<Am/V<15 |
| | -0.6761 | 50.7910 | -40.0000 | 15<Am/V<30 |
| R120 | 0.8283 | 57.6550 | -15.0000 | 14<Am/V<30 |
| | 0.0000 | 1.5708 | 480.0000 | 14<Am/V<30 |

### 4-4- Fire effect on the concrete component

The effect of the fire on the concrete was determined by the 500 ºC isothermal [1]. The external layer of concrete to be neglected may be calculated in both principal directions, defining $b_{c,fi,v}$ and $b_{c,fi,h}$. According to Eurocode EN1994 1.2 [1], the thickness of concrete to be neglected depends on section factor $A_m/V$, for standard fire

resistance classes of R90 and R120. The new proposal demonstrates a strong dependence on the section factor for all fire rating.

Fig. 26 present the new proposal for $b_{c,fi,v}$ and $b_{c,fi,h}$ for HEB and IPE sections.

Table 21 and Table 22 provide the new formulae to determine the thickness of concrete to be neglected in fire design, based on the new Eq.(50), which applies to both cross section types (HEB and IPE) and directions (horizontal and vertical).

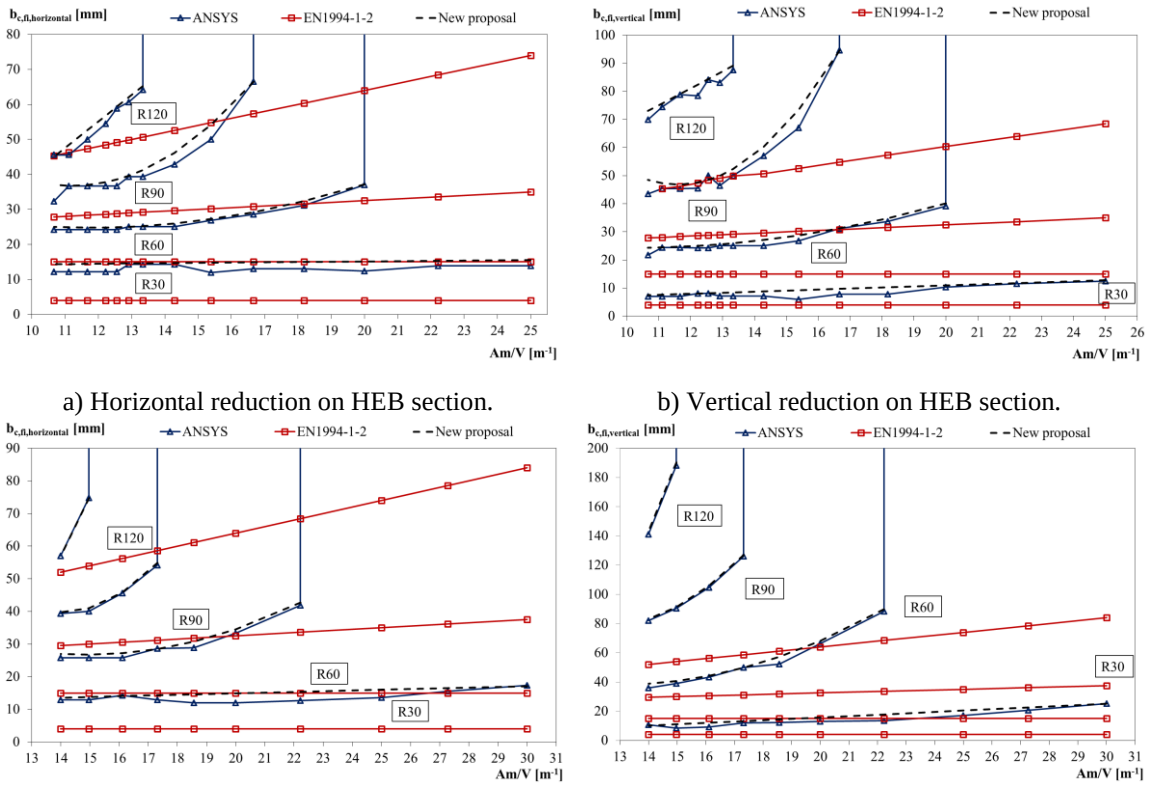


a) Horizontal reduction on HEB section.

b) Vertical reduction on HEB section.

c) Horizontal reduction on IPE section.

d) Vertical reduction on IPE section.

Fig. 26 - Thickness reduction of the concrete area for HEB and IPE sections.

The new proposal defines the amount of concrete to be neglected in both principal directions. This value depends on the section factor for every fire rating class.

$$b_{c,fi} = a \times \left(A_m / V\right)^2 + b \times A_m / V + c \tag{50}$$

Table 20 - Reduction in thickness of the concrete (HEB).

| | $b_{c,\,fi} = a \times (A_m/V)^2 + b \times A_m/V + c$ | | | | | | |
|---|---|---|---|---|---|---|---|
| | $b_{c,\,fi,horizontal}$ | | | $b_{c,\,fi,vertical}$ | | | |
| Resistance Standard fire | a | b | c | a | b | c | Section factor |
| R30 | 0,0 | 0,0809 | 13,5 | 0,0 | 0,372 | 3,5 | $10 < A_m/V < 25$ |
| R60 | 0,1825 | -4,2903 | 50,0 | 0,1624 | -3,2923 | 41,0 | $10 < A_m/V < 20$ |
| R90 | 1,0052 | -22,575 | 163,5 | 1,8649 | -43,287 | 298,0 | $10 < A_m/V < 17$ |
| R120 | 0,0 | 7,5529 | -35,5 | 0,0 | 6,0049 | 9,0 | $10 < A_m/V < 13$ |

Table 21 - Reduction in thickness of the concrete (IPE).

| | $b_{c,\,fi} = a \times (A_m/V)^2 + b \times A_m/V + c$ | | | | | | |
|---|---|---|---|---|---|---|---|
| | $b_{c,\,fi,horizontal}$ | | | $b_{c,\,fi,vertical}$ | | | |
| Resistance Standard fire | a | b | c | a | b | c | Section factor |
| R30 | 0,0 | 0,2206 | 10,5 | 0,0 | 0,9383 | -3,0 | $14 < A_m/V < 30$ |
| R60 | 0,2984 | -8,8924 | 93,0 | 0,5888 | -15,116 | 135,0 | $14 < A_m/V < 22$ |
| R90 | 1,3897 | -38,972 | 313,0 | 2,0403 | -50,693 | 393,0 | $14 < A_m/V < 17$ |
| R120 | 0,0 | 18,283 | -199,0 | 0,0 | 48,59 | -537,0 | $14 < A_m/V < 15$ |

Fig. 27 The new proposal introduces a parametric approximation, based on the standard fire resistance and section factor, Eqs.(51)-(52). The application limits are presented in Table 22.

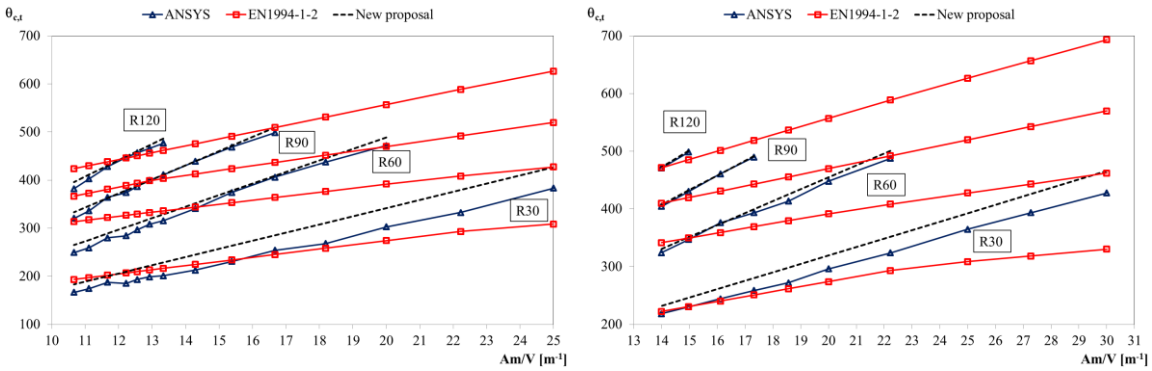


a) HEB sections b) IPE section

Fig. 27 - Average temperature of residual concrete.

$$\theta_{c,t} = 3.1 \times t^{0.5} \times (A_m/V) + 0.003 \times t^{1.95} \quad (51)$$

$$\theta_{c,t} = 2.67 \times t^{0.5} \times (A_m/V) + 3.4 \times t^{0.61} \quad (52)$$

Table 22 - Application limits for average temperature of the concrete.

| Standard fire resistance class | Section factor (HEB) | Section factor (IPE) |
|---|---|---|
| R30 | Am/V<25 | Am/V<30 |
| R60 | Am/V<20 | Am/V<23 |
| R90 | Am/V<17 | Am/V<18 |
| R120 | Am/V<14 | Am/V<15 |

### 4-5- Fire effect on the reinforcement component

The effect of the fire into the reinforcement depends on the calculation of the average temperature of the material. The new parametric formula may be used to determine this effect.

Fig. 28 depicts the average temperature of rebars determined by the numerical results. The results of the current version of Eurocode EN1994-1-2 [1] were indirectly determined through the most critical reduction factor. Alternatively, the new parametric formula is presented for the calculation of the average temperature of rebars. Eqs.(53)-(54) were developed to the new proposal, based on the distance between rebars exposed surface (u), fire rating class (t) and section factor $A_m/V$.

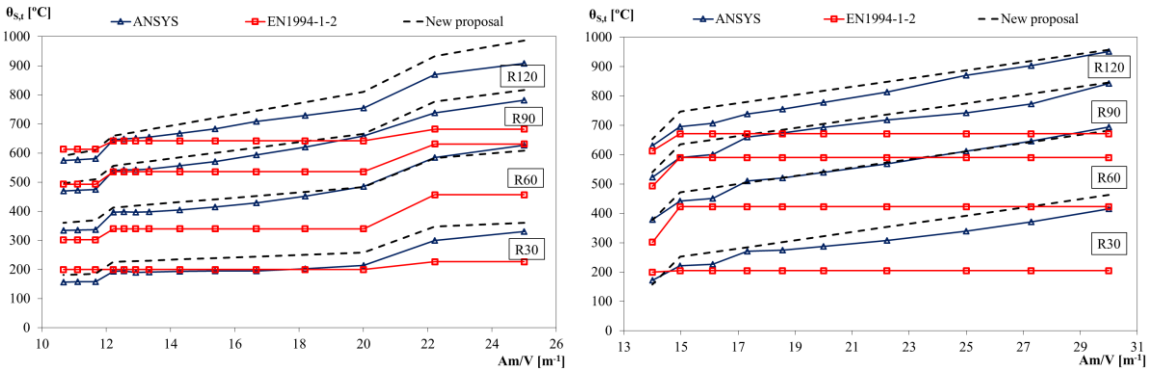


a) HEB sections b) IPE section

Fig. 28 - Average temperature of rebars. HEB sections (left). IPE Sections (right).

$$\theta_{s,t} = 0.1\times t^{1.1}\times\left(A_m/V\right)+7.5\times t-0.1\times t^{1.765}-8\times u+390 \quad ,(HEB) \tag{53}$$

$$\theta_{s,t} = 14.0\times\left(A_m/V\right)+11.0\times t-0.1\times t^{1.795}-8\times u+115 \quad ,(IPE) \tag{54}$$

This page was intentionally left in blank

# CHAPTER.5 NUMERICAL SOLUTION METHOD

This chapter defines the numerical simulation method used for the buckling analysis of Partially Encased Columns. This simulations method is based on a four steps procedure. The first step solves the nonlinear transient thermal analysis to define the temperature of the elements under fire. The second step considers a static and Eigen buckling analysis to define the elastic buckling resistance for specific fire rating classes (30 and 60 minutes). The third step considers the nonlinear incremental solution method to find the plastic resistance of the cross section for specific fire rating classes (30 and 60 minutes). The finally step considers the nonlinear incremental solution method to find the buckling resistance of partially encased columns for specific fire rating periods (30 and 60 minutes). The model is a full three dimensional model, based on perfect contact between materials.

## 5-1- Elements used in numerical models

Different types of elements are going to be applied to solve the thermal and the mechanical analysis. These elements are defined in the data base of the software ANSYS. The elements were selected according to the simulation needs, using the lower order finite elements available.

### 5-1-1- Thermal model

Solid 70 has a 3D thermal conduction capability, the element has 8 nodes with a single degree of freedom, temperature, at each node. The element is used to a 3-D, transient thermal analysis see Fig. 29. The element also can compensate for mass transport heat flow from a constant velocity field, [28].

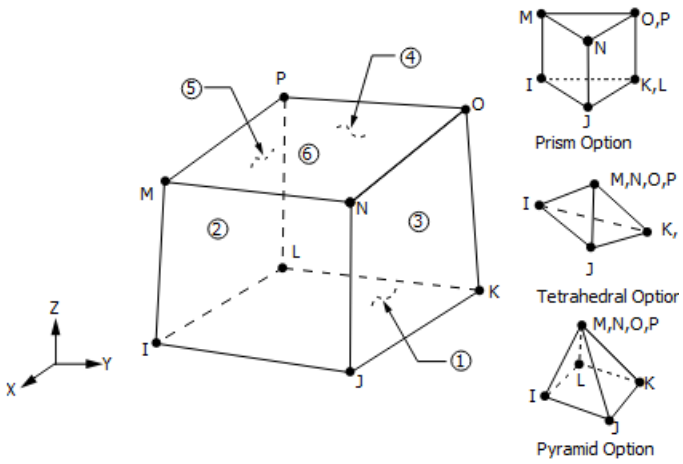


Fig. 29 - SOLID70 Geometry (ANSYS16.2).

The element uses linear interpolating functions, but is able to use 2x2x2 integration point (full integration), [28]. This element is going to be applied to the volume material of steel and concrete.

LINK33 is a uniaxial element with the ability to conduct heat between its nodes. The element has a single degree of freedom, temperature, at each node see Fig. 30. The conducting bar is applicable to the transient thermal analysis, [28].

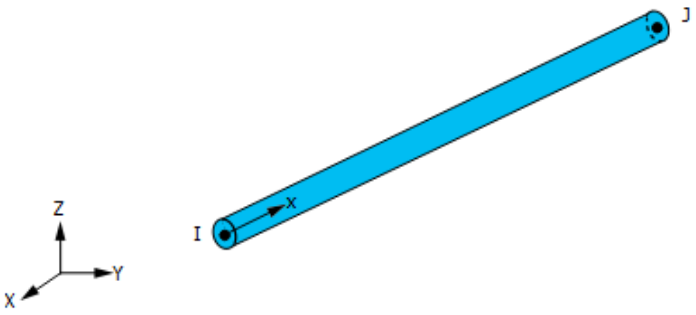


Fig. 30 - LINK33 Geometry (ANSYS16.2).

The element uses linear interpolating functions and only 1 integration point [28]. This element is going to be used to model the reinforcement.

### 5-1-2- Structural model

Solid 185 is a 3D modelling element used for structures, is defined by 8 nodes, each has 3 degrees of freedom (translation in each direction of the coordinates systems). The element is able to work in elastic, plastic and large deflection, [28].

Fig. 31 represents the geometry of the finite element and the out surfaces used to apply the boundary conditions. This figure also represents some modified configurations that were avoided.

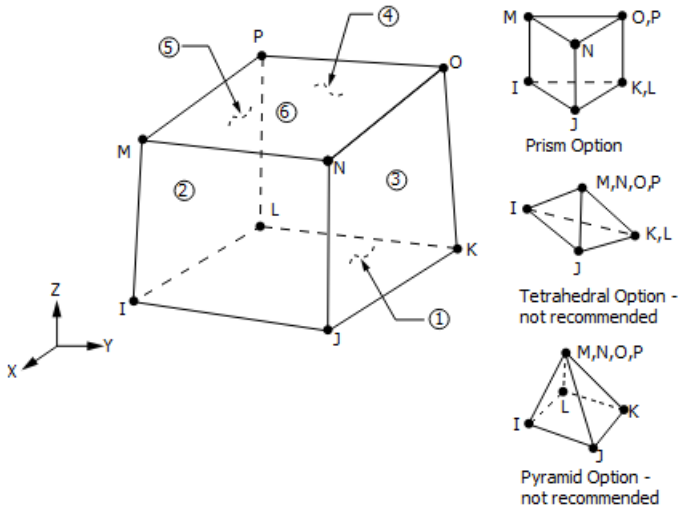


Fig. 31 - SOLID185 Geometry (ANSYS16.2).

This element uses linear interpolating function, but is able to use 2x2x2 integration points (full integration) or 1 integration points (reduced integration), [28]. This element is going to be used to model the steel hot rolled profile.

Link 180 is a 3D spar that can model trusses and bars. The element is a uniaxial tension compression with 3 degrees of freedom in each node (translations in each direction of coordinate system) see Fig. 32. The element is able to work in elastic, plastic and large deflection, [28].

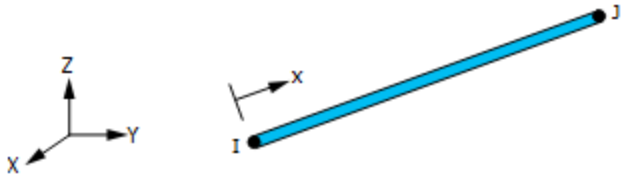


Fig. 32 - LINK180 Geometry (ANSYS 16.2).

The element uses linear interpolating functions and only 1 integration point [28]. This element is going to be used to model the reinforcement.

SOLID65 is used for the 3-D modelling of solids with or without reinforcing bars (rebar). The solid is capable of cracking in tension and crushing in compression. The element is defined by eight nodes having three degrees of freedom at each node: translations in the nodal x, y, and z directions. Up to three different rebar specifications can be defined see Fig. 33.

The concrete is capable of cracking (in three orthogonal directions), crushing and achieve plastic deformation. The rebar are capable of tension and compression, but not able to resist shear [28].

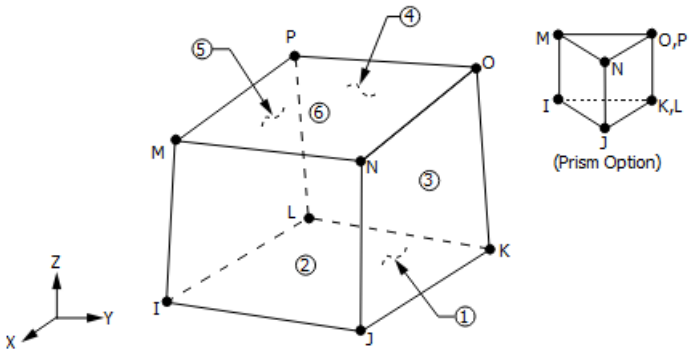


Fig. 33 - Solid65 Geometry (ANSYS 16.2).

The element uses linear interpolating function, but is able to use 2x2x2 integration points (full integration), [28]. This element is going to use to model the concrete part of the PEC.

### 5-2- Convergence test

To know the best mesh applied to the PEC a convergence test of the solution was done with different sizes in Z direction. Current mesh considers 50 element divisions for height of 3m columns and 80 element divisions for height of 5m columns. The size of the mesh applied to the cross section was based on a previous experience of the simulation for 2D analysis [23].

### 5-3- Thermal analysis

The first step considers the nonlinear transient thermal analysis to calculate the temperature field. The finite element method requires the solution of Eq. (55) in the internal domain of the partially encased column and Eq. (56) in the external surface, when exposed to fire. In these equations: $T$ represents the temperature of each material; $\rho(T)$ defines the specific mass; $C_p(T)$ defines the specific heat; $\lambda(T)$ defines the thermal conductivity; $\alpha_c$ specifies the convection coefficient; $T_g$ represents the gas temperature of the fire compartment, using standard fire ISO 834 [4] around the cross section (4 exposed sides); $\Phi$ specifies the view factor; $\varepsilon_m$ represents the emissivity of each material; $\varepsilon_f$ specifies the emissivity of the fire; $\sigma$ represents the Stefan-Boltzmann constant.

$$\nabla \cdot (\lambda_{(T)} \cdot \nabla T) = \rho_{(T)} \cdot C_{p(T)} \cdot \partial T / \partial t \qquad (\Omega) \tag{55}$$

$$(\lambda_{(T)} \cdot \nabla T) \cdot \vec{n} = \alpha_c (T_g - T) + \Phi \cdot \varepsilon_m \varepsilon_f \cdot \sigma \cdot (T_g^4 - T^4) \qquad (\partial\Omega) \tag{56}$$

The three-dimensional model uses element SOLID70 and element LINK33 to model the profile / concrete and rebars, which are presented before.

The nonlinear transient thermal analysis was defined with an integration time step of 60 s, which can decrease to 1 s and increase up to 120 s. The criterion for convergence uses a tolerance value of the heat flow, smaller than 0.1% with a minimum reference value of $1x10^{-6}$.

The temperature field was determined for the total time of 7200 s. Fig. 34 shows an example of the partially encased column exposed to ISO834 fire [4], after 30 and 60 minutes. The temperature field was recorded for the corresponding resistance class and applied as body load to the mechanical model. The mesh was defined after a solution convergence test.

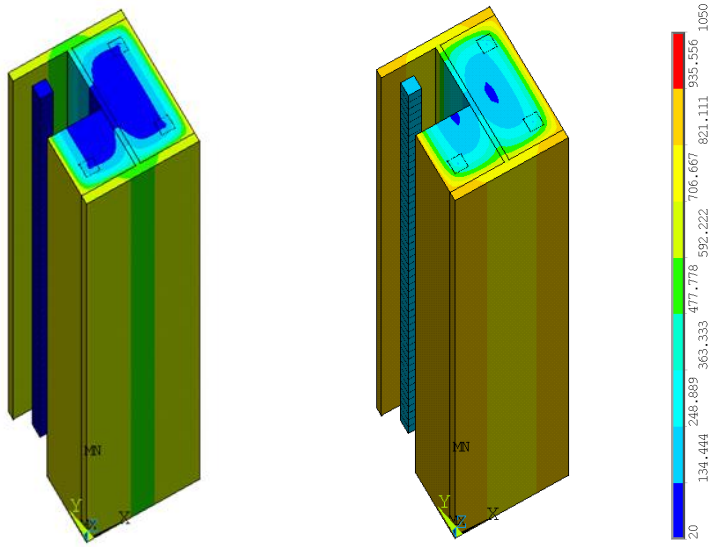


a) Time=30 min. b) Time=60 min.

Fig. 34 - Numerical thermal results for column HEB 360.

Table 23 presents the thermal results from ANSYS, with min and max value. The minimum temperature of profile decrease when the cross sections increase, mainly due to the decrease of the section factor. The results of the thermal analysis are presented in Annex.

Table 23 – Thermal results from ANSYS [°C].

| Profile | $A_m/V$ | R30 | R60 | R90 | R120 |
|---|---|---|---|---|---|
| HEB160 | 25,00 | 269-801 | 566-934 | 722-1000 | 823-1045 |
| HEB180 | 22,22 | 214-801 | 498-933 | 677-1000 | 774-1044 |
| HEB200 | 20,00 | 136-800 | 394-932 | 565-999 | 683-1045 |
| HEB220 | 18,18 | 115-799 | 342-932 | 502-999 | 621-1044 |
| HEB240 | 16,67 | 101-799 | 299-931 | 467-999 | 596-1044 |
| HEB260 | 15,38 | 89-799 | 246-931 | 406-998 | 532-1044 |
| HEB280 | 14,29 | 76-798 | 196-930 | 357-998 | 481-1044 |
| HEB300 | 13,33 | 63-798 | 153-930 | 313-998 | 432-1044 |
| HEB320 | 12,92 | 60-796 | 142-929 | 294-998 | 413-1046 |
| HEB340 | 12,55 | 57-795 | 134-929 | 278-998 | 394-1043 |
| HEB360 | 12,22 | 55-794 | 128-928 | 263-997 | 379-1043 |
| HEB400 | 11,67 | 49-793 | 119-928 | 238-997 | 350-1043 |
| HEB450 | 11,11 | 44-792 | 109-927 | 206-997 | 316-1043 |
| HEB500 | 10,67 | 40-790 | 103-926 | 178-997 | 287-1043 |
| IPE200 | 30,00 | 363-807 | 641-936 | 744-1001 | 892-1046 |
| IPE220 | 27,27 | 272-806 | 535-935 | 686-1001 | 740-1045 |
| IPE240 | 25,00 | 253-804 | 511-934 | 667-1000 | 734-1045 |
| IPE270 | 22,22 | 193-804 | 437-934 | 596-1000 | 700-1045 |
| IPE300 | 20,00 | 142-803 | 391-933 | 563-999 | 672-1045 |
| IPE330 | 18,56 | 118-802 | 344-933 | 512-999 | 636-1045 |
| IPE360 | 17,32 | 105-801 | 300-932 | 463-999 | 588-1044 |
| IPE400 | 16,11 | 94-800 | 253-931 | 410-998 | 533-1044 |
| IPE450 | 14,97 | 81-800 | 212-931 | 363-998 | 482-1044 |
| IPE500 | 14,00 | 54-798 | 160-930 | 310-998 | 427-1043 |

### 5-4- Eigen buckling analysis

The static linear analysis is the basis for the eigen buckling analysis. The solution of Eq. (57) must be find primarily, assuming $\{F_{ref}\}$ is an arbitrary load to be aplied on the Partially Encased Column (usually a unit force). $[K]$ is its stiffness matrix and $\{d\}$ is the displacement vector. When the displacements are known, the stress field can be calculated for the reference load $\{F_{ref}\}$, which can be used to form the stress stiffness matrix $[K_{\sigma,ref}]$. Since the stress stiffness matrix is proportional to the load vector $\{F_{ref}\}$, an arbitrary stress stiffness matrix $[K_{\sigma}]$ and an arbitrary load vector $\{F\}$ may be defined by a constant $\lambda$ as shown by Eqs. (58)-(59).

The stiffness matrix is not changed by the applied load because the solution is linear. A relation between the stiffness matrices, the displacement and the critical load can then be presented as in Eq(60), which can be used to predict the bifurcation point. The critical load is defined as $\{F_{cri}\}$. Since the buckling mode is defined as a change in displacement for the same load, Eqs.(60-(61) are still valid, where $\{\delta d\}$ represents the incremental buckling displacement vector. The difference between Eq.(60) and Eq.(61) produces an eigenvalue problem, represented by Eq.(62) Where the smallest root defines the first buckling load, when bifurcation is expected.

$$[K]\{d\} = \{F_{ref}\} \tag{57}$$

$$[K_{\sigma}] = \lambda[K_{\sigma,ref}] \tag{58}$$

$$\{F\} = \lambda\{F_{ref}\} \tag{59}$$

$$\left[[K] + \lambda_{cri}[K_{\sigma,ref}]\right]\{d\} = \lambda_{cri}\{F_{ref}\} \tag{60}$$

$$\left[[K] + \lambda_{cri}[K_{\sigma,ref}]\right]\{\{d\} + \{\delta d\}\} = \lambda_{cri}\{F_{ref}\} \tag{61}$$

$$\left[[K] + \lambda\,[K_{\sigma,ref}]\right]\{\delta d\} = \{0\} \tag{62}$$

Fig. 35 presents the elastic modulus used for all materials used in the buckling analysis.

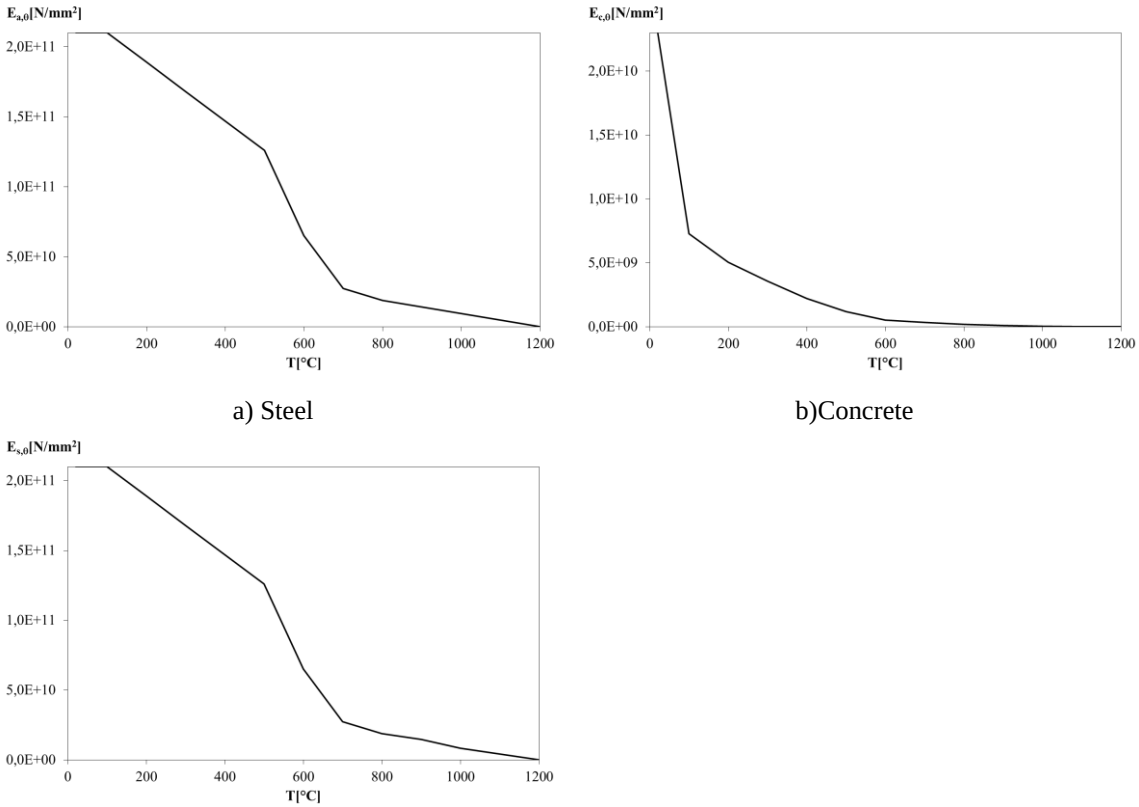


a) Steel

b)Concrete

c)Reinforcement

Fig. 35 - Elastic modulus for the three materials.

The trivial solution is not of interest, which means that the solution for $\lambda$ is define for an algebraic equation, imposing the determinant of the global matrix equal to zero. The calculated eigenvalue is always related to an eigenvector $\{\delta d\}$ called a buckling mode shape, see Fig. 36.

This numerical solution of a linear buckling analysis assumes that everything is perfect and therefore the real buckling load will be lower than the calculated buckling load if the imperfections are taking into account.

*a) IPE330, after 30 min.*

*b) HEB160 after 60 min*

Fig. 36 - Example of Buckling shape for different fire ratings classes.

Table 24 and Table 25 presents the results of elastic critical load for both 3m and 5m of height. The highlighted cells in red colour means that, under this conditions (buckling length and fire rating), PEC does not attained buckling mode of instability as a potential failure mode.

Table 24 - Elastic critical load for 3m height.

| | $N_{fi,cr,z}\,numeric\,[N]$ | | | | | |
|---|---|---|---|---|---|---|
| | R30 | | | R60 | | |
| Profile | 0.5L | 0.7L | 1.0L | 0.5L | 0.7L | 1.0L |
| HEB160 | 1535090 | 782942 | 396994 | 846567 | 454020 | 205250 |
| HEB180 | 2861160 | 1665830 | 747883 | 1271250 | 764504 | 350580 |
| HEB200 | 5495730 | 3355210 | 1548000 | 2632530 | 1734060 | 841110 |
| HEB220 | 10001900 | 5774740 | 2815480 | 5067910 | 3209930 | 1657820 |
| HEB240 | 14194900 | 8216710 | 4022230 | 7350300 | 4636390 | 2389160 |
| HEB260 | 25820400 | 14158300 | 7048640 | 11515500 | 8488580 | 4523700 |
| HEB280 | 27464700 | 18907400 | 9220030 | | 11334400 | 5981060 |
| HEB300 | | 24153000 | 12069300 | | 14307300 | 7596240 |
| HEB320 | | 25891800 | 12804200 | | | 7877420 |
| HEB340 | | | 16759200 | | | 10753400 |
| HEB360 | | | 17477100 | | | 11227000 |
| HEB400 | | | 18768300 | | | 12156600 |
| HEB450 | | | 20405500 | | | 12272200 |
| HEB500 | | | 22057500 | | | 13348100 |
| IPE200 | 238975 | 117396 | 57444 | 106430 | 52505 | 25706 |
| IPE220 | 510524 | 265186 | 131205 | 231074 | 128115 | 65163 |
| IPE240 | 814784 | 429479 | 213145 | 379842 | 217457 | 111601 |
| IPE270 | 1659240 | 976825 | 493195 | 816836 | 537389 | 286241 |
| IPE300 | 2765470 | 1583390 | 802937 | 1401830 | 893276 | 475473 |
| IPE330 | 3761010 | 2153980 | 1086170 | 1938540 | 1228040 | 646651 |
| IPE360 | 6300380 | 3806060 | 1969010 | 2669680 | 2291210 | 1259700 |
| IPE400 | 9025840 | 4966800 | 2550860 | 5151120 | 3142400 | 1691770 |
| IPE450 | 11508900 | 6259790 | 3216870 | 6604230 | 3960080 | 2164200 |
| IPE500 | 16789000 | 9621320 | 5068080 | 8955800 | 5658900 | 3163470 |

Table 25 - Elastic critical load for 5m height.

| | $N_{fi,cr,z}numeric[N]$ | | | | | |
|---|---|---|---|---|---|---|
| | R30 | | | R60 | | |
| Profile | 05L | 07L | 10L | 05L | 07L | 10L |
| HEB160 | 662244 | 340583 | 164521 | 295117 | 154634 | 75056 |
| HEB180 | 1104620 | 570139 | 275688 | 504631 | 267618 | 130256 |
| HEB200 | 2175030 | 1160140 | 565971 | 1081920 | 610951 | 302453 |
| HEB220 | 3915170 | 2161300 | 1062430 | 2127850 | 1277060 | 641646 |
| HEB240 | 5384540 | 2985160 | 1481450 | 2981870 | 1785420 | 902212 |
| HEB260 | 9595780 | 5412950 | 2706980 | 5679270 | 3508970 | 1799750 |
| HEB280 | 12345800 | 7223840 | 3594570 | 7513210 | 4612230 | 2353450 |
| HEB300 | 16267700 | 9514200 | 4563120 | 9256760 | 5930490 | 3020250 |
| HEB320 | 18604000 | 10184500 | 4861940 | 10967000 | 6252800 | 3645640 |
| HEB340 | 24848800 | 13614800 | 6479700 | 13262800 | 7625230 | 3732410 |
| HEB360 | 27522400 | 14184200 | 6725040 | 14498700 | 7850640 | 3828470 |
| HEB400 | 26938500 | 15279500 | 7176420 | 16067700 | 9828650 | 4831790 |
| HEB450 | 29545400 | 15881800 | 7747740 | 17087200 | 9973030 | 5039440 |
| HEB500 | 32276500 | 17204000 | 8361930 | 18060000 | 10418100 | 5240600 |
| IPE200 | 86498 | 42247 | 20641 | 38655 | 18920 | 9250 |
| IPE220 | 190131 | 95940 | 47105 | 88209 | 46276 | 22949 |
| IPE240 | 312800 | 159011 | 78106 | 155336 | 83803 | 41759 |
| IPE270 | 690296 | 365205 | 180554 | 370319 | 214142 | 108307 |
| IPE300 | 1118920 | 596274 | 294632 | 614216 | 355941 | 176678 |
| IPE330 | 1508040 | 804849 | 398230 | 838272 | 483233 | 243539 |
| IPE360 | 2609880 | 1461990 | 730561 | 1534950 | 946323 | 485853 |
| IPE400 | 3419020 | 1902320 | 948095 | 2104890 | 1271350 | 646605 |
| IPE450 | 4310130 | 2391610 | 1192070 | 2661540 | 1593970 | 809801 |
| IPE500 | 6607140 | 4050130 | 2042400 | 4222540 | 2836860 | 1470670 |

### 5-5- Non-linear plastic resistance

A similar 3D model to 2nd step (eigen buckling analysis) was used for the calculation of the plastic resistance but with geometrical and material nonlinear analysis. Also different boundary condition were applied to model to prevent any kind of instability. This simulation was based on the incremental displacement in vertical direction and iterative solution method (Newton Raphson). Typical incremental displacement of 0,1 mm was applied, adjusting to any minimum incremental displacement of 0,01 mm and to maximum incremental displacement of 0,2 mm. The criterion for convergence is based on displacement with tolerance value of 5%. Plastic resistance is defined by the reaction force when the reinforcement attains plastic strain. This was the criterion selected to define the plastic resistance of the cross section.

Fig. 37 presents the materials properties used in finite elements for the non-linear plastic resistance.

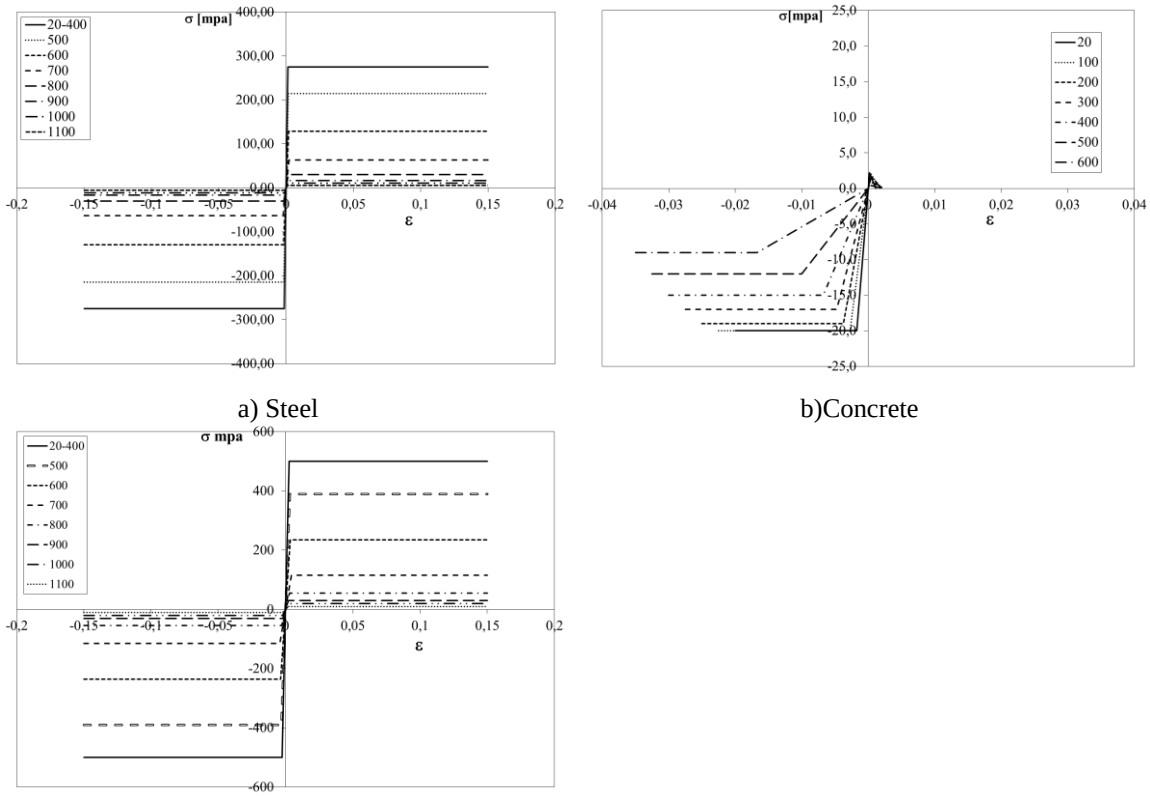


a) Steel

b)Concrete

c)Reinforcement

Fig. 37 - Curve stress-strain of steel, concrete and reinforcement.

Fig. 38 presents the plastic strain of HEB360 and curve of stress-strain used to explain know plasticity takes place in each material of PEC.

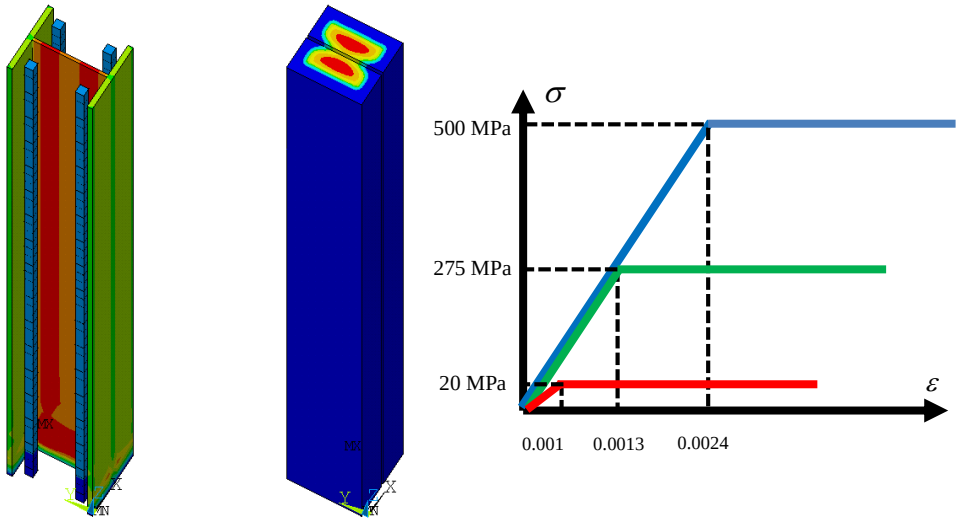


Fig. 38 - Plastic straine of HEB360 for R30.

Table 26 presents the results of plastic resistance to axial compression at elevated temperature, obtained from numerical simulation model.

Table 26 - Plastic resistance to axial compression ANSYS.

| | $N_{fi,pl,Rd}numeric[N]$ | |
|---|---|---|
| Profile | R30 | R60 |
| HEB160 | 2198200 | 1347500 |
| HEB180 | 2757100 | 1818000 |
| HEB200 | 3744700 | 2036700 |
| HEB220 | 4731800 | 3508200 |
| HEB240 | 5447200 | 5024300 |
| HEB260 | 6705000 | 6182000 |
| HEB280 | 7994700 | 6378800 |
| HEB300 | 8818500 | 7193500 |
| HEB320 | 8539100 | 7711740 |
| HEB340 | 9923700 | 9154000 |
| HEB360 | 10401000 | 9560000 |
| HEB400 | 11262000 | 10362000 |
| HEB450 | 12315000 | 11356000 |
| HEB500 | 13372000 | 12346000 |
| IPE200 | 1305900 | 814720 |
| IPE220 | 1930700 | 1496100 |
| IPE240 | 2165700 | 1739900 |
| IPE270 | 2868400 | 2487600 |
| IPE300 | 3309700 | 2861000 |
| IPE330 | 3734700 | 3201500 |
| IPE360 | 4885000 | 4329900 |
| IPE400 | 5472500 | 4860900 |
| IPE450 | 6177900 | 5458000 |
| IPE500 | 8008900 | 7049500 |

### 5-6- Non-linear Buckling analysis

The 3D model of 2nd step (eigen buckling analysis) was modified to include the geometric imperfections. The geometric imperfections were defined based on the instability mode shape defined in the elastic buckling analysis. This solution method is incremental and iterative (Newton Raphson). Typical incremental displacement of 0,1 mm was applied, with minimum incremental displacement of 0,01 mm and maximum incremental displacement of 0,2 mm. The criterion for convergence is based on displacement with tolerance value of 5%. Eigenvalue buckling analysis predicts the theoretical buckling strength (the bifurcation point) of an ideal linear elastic structure. However, imperfections and nonlinearities prevent most real- world structures from achieving their theoretical elastic buckling strength. The nonlinear buckling analysis is a static analysis with large deflection (equilibrium in deformed configuration), extended

to a point where the structure reaches its ultimate limit state (plasticity, modification into a mechanism). The buckling load it's maximum load determined for the curve plotted for load displacement curve.

Fig. 39 presents buckling mode of HEB240 and IPE330 for different fire ratings classes (3m of height). Typical curve used for force displacement is also represented.

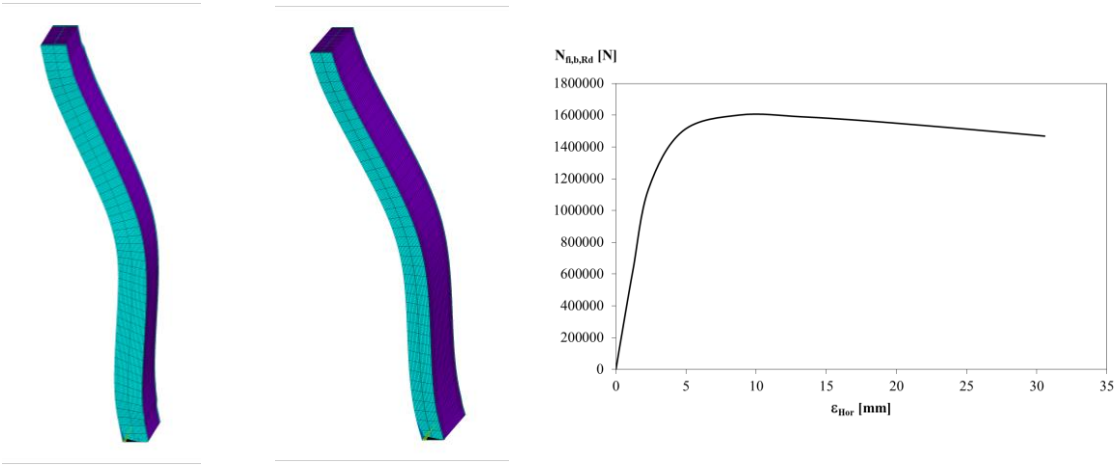


*a) HEB240, after 30min.* *b) IPE330, after 60min.* *c) Vertical displacement load.*

Fig. 39 - Buckling mode of HEB240 and IPE330 for different fire ratings classes.

Table 27 presents the results of buckling load for both 3m and 5m of height and boundary condition 0,5L. The highlighted cells in red colour means that, under this conditions (buckling length and fire rating), PEC does not attained buckling mode of instability as a potential failure mode.

Table 27 - Buckling resistance from ANSYS.

| | | $N_{fi,b,Rd}numeric[N]$ | | | |
|---|---|---|---|---|---|
| | | 3m | | 5m | |
| Profile | $A_m/V$ | R30 | R60 | R30 | R60 |
| HEB160 | 25,00 | 1625700 | 1601100 | 1207800 | 1132900 |
| HEB180 | 22,22 | 2093500 | 2019900 | 1618700 | 1518200 |
| HEB200 | 20,00 | 2840400 | 2779000 | 2298100 | 2180700 |
| HEB220 | 18,18 | 3645000 | 3583900 | 3055000 | 2924700 |
| HEB240 | 16,67 | 4213300 | 4154700 | 3622400 | 3468000 |
| HEB260 | 15,38 | 5252500 | 5195900 | 4639400 | 3707100 |
| HEB280 | 14,29 | 5823500 | | 5260100 | 4489700 |
| HEB300 | 13,33 | | | 5865400 | 5094800 |
| HEB320 | 12,92 | | | 6257400 | 6092700 |
| HEB340 | 12,55 | | | 7336000 | 7189300 |
| HEB360 | 12,22 | | | 7668600 | 7522200 |
| HEB400 | 11,67 | | | 8565500 | 8210400 |
| HEB450 | 11,11 | | | 8904600 | 8747400 |
| HEB500 | 10,67 | | | 9613900 | 9442600 |
| IPE200 | 30,00 | 764090 | 682200 | 355810 | 328890 |
| IPE220 | 27,27 | 1198900 | 1033100 | 542680 | 497550 |
| IPE240 | 25,00 | 1408200 | 1321000 | 733740 | 671740 |
| IPE270 | 22,22 | 2001400 | 1919800 | 1167100 | 1069500 |
| IPE300 | 20,00 | 2444700 | 2369500 | 1612000 | 1487000 |
| IPE330 | 18,56 | 2822000 | 2747600 | 1982500 | 1825400 |
| IPE360 | 17,32 | 3709200 | 3630400 | 2768700 | 2592800 |
| IPE400 | 16,11 | 4213200 | 4200000 | 3559800 | 3061100 |
| IPE450 | 14,97 | 4794300 | 4759800 | 3811900 | 3588700 |
| IPE500 | 14,00 | 6283600 | 6454100 | 4122300 | 4863900 |

# CHAPTER.6 COMPARISON OF RESULTS

Fig. 40 presents the comparison of the buckling curve, using the results from the new proposal and results from the Eurocode EN1993-1-1 [2], for 30,60,90 and 90 minutes of fire exposure and for different boundary condition. The results where plotted using buckling curve C.

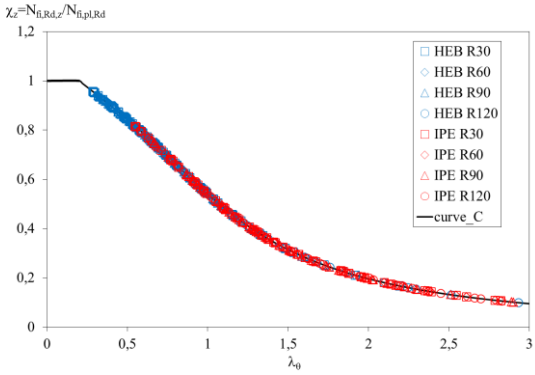


Fig. 40 - Buckling curve using new formulae.

Fig 41 and Fig 42 presents the comparison of the buckling load, using the results from the new proposal and results from the numerical solution, for 30 and 60 minutes of fire exposure and for different boundary condition. The ratio between the critical load and the axial plastic resistance depends on the non-dimensional slenderness ratio $\overline{\lambda}_{\vartheta}$.

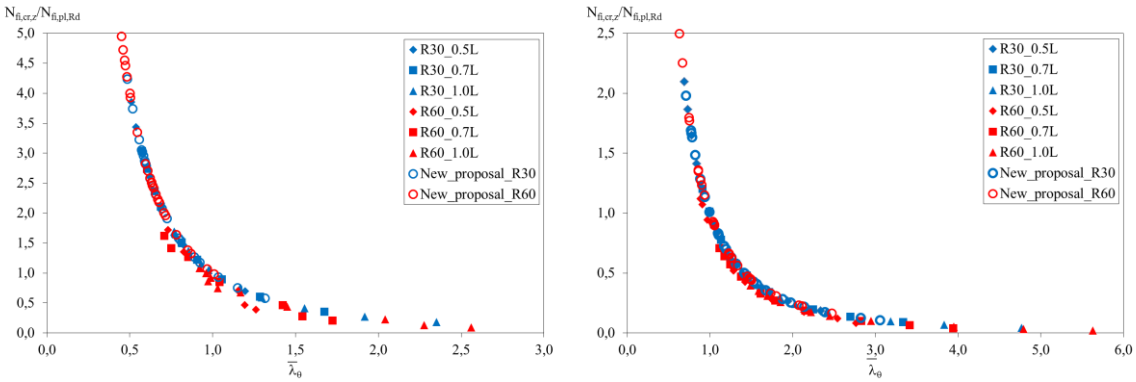


*a) HEB Profile.* *b) IPE Profile.*

Fig. 41 - Ratio between critical and plastic resistance for 3m of height.

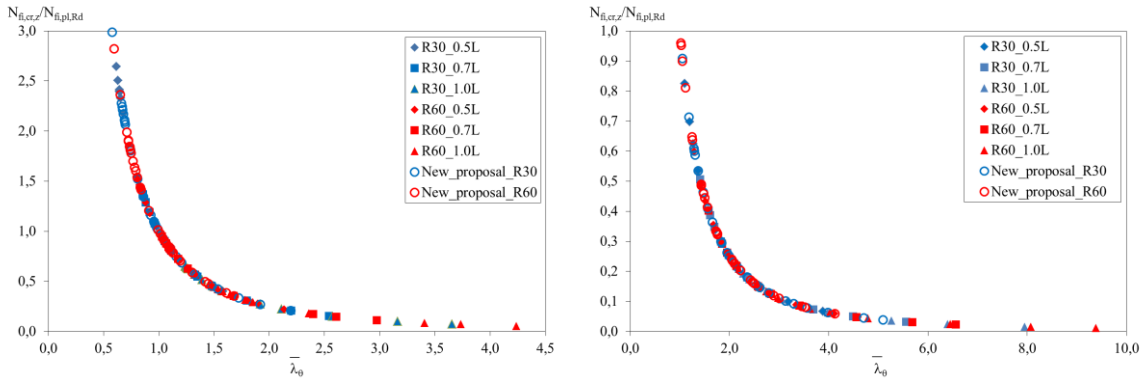


*a) HEB Profile.* *b) IPE Profile.*

Fig. 42 - Ratio between critical and plastic resistance for 5m of height.

The numerical solution method is based on the elastic buckling analysis, considering the resistance of the four components, taking into account the update of the material properties and the full geometry of column. This fact justifies that the numerical results are always higher that the ones presented by the new formulae [29].

Fig. 43 presents the comparison of the buckling curve, using the results from Eurocode EN 1993-1-1 [2] and results from the non-linear buckling numerical solution, for 30 and 60 minutes of fire exposure and for buckling length $L_\theta = 0{,}5L$. This buckling length was used because bad results were obtained to the other buckling length $L_\theta = 0{,}7L$ and $1{,}0L$ related to the concentration effect of load in selected nodes (localised effect).

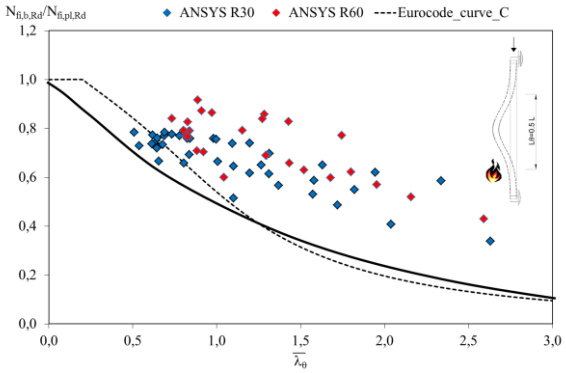


Fig. 43 - Buckling curve (comparison between ANSYS and Eurocode).

This numerical solution method is based on the buckling analysis, considering the resistance of the four components, taking into account the update of the material

properties and the full geometry of column. This fact justifies that the numerical results are also higher that the ones presented by the Eurocode.

This page was intentionally left in blank

# CHAPTER.7 CONCLUSIONS

The buckling analysis of partially encased column was analysed at room temperature and under fire conditions. Two different solution methods were applied to define the buckling resistance of partially encased columns in case of fire. The simplified method proposed in Annex G EN1994-1-2 [1] with new proposal formulae. The current proposal of Eurocode (simple calculation method) is unsafe when compared to the numerical results.

The results of new proposal is based on the balanced summation method, proposed to modify the current version of Eurocode 4 part 1.2 [1], but using safer formulas for the balanced summation model, based on the evolution of the average temperature in the flange, based on the residual height of the web according to 400 º C isothermal criterion, based on the reduction of concrete and also the average temperature according to 500 ºC isothermal criterion, and finally based on the average temperature of the reinforcement.

The numerical solution method is based on the elastic buckling analysis, considering the full resistance of the four components, updating the material properties and the full geometry of column. This fact justifies that the numerical results are always higher that the ones presented by the new formulae, and also it was found that the numerical results is conservative for R30 and R60 exposure class, being unsafe for the other classes of fire resistance.

In this study there was a significant difference between the buckling values obtained by the simple calculation method and the numerical results. The difference may be related to the hypothesis of the finite element model, used for this study. These results are going to be considered in the final step of this investigation to define the buckling resistance of PEC and validate the best curve to fit the results.

Partially encased column presents higher buckling resistance than bare steel columns. Is was also verified that the buckling resistance decreases with the buckling length and for higher fire rating classes, smaller buckling loads are expected.

According to the elastic buckling results, good agreement was found between the new proposal and the numerical simulation, concluding that the new proposal is safe.

The material and geometric non-linear analysis revealed that the buckling curve suggested by Eurocode is not safe and a different curve fit should be proposed.

This study must be extended for other types of cross section and different configurations of PEC. Experimental tests are also required to validate the best curve to fit the results.

## REFERENCES

[1] CEN - EN 1994-1-2; “Eurocode 4 - Design of composite steel and concrete structures- Part 1-2: General rules - Structural fire design”; Brussels, August 2005.

[2] CEN - EN 1993-1-1; “Eurocode 3: Design of steel structures - Part 1-1: General rules - Rules for buildings.”, European standards; Brussels, 2005.

[3] Ministry of Internal Affairs, Decree No. 1532/2008, Technical regulation of fire safety in buildings (in Portuguese), December 29, 2008.

[4] ISO 834-1. “Fire-resistance tests - Elements of building construction – Part 1: general requirements”. 1999.

[5] Malhotra H.L. and Stevens “Fire resistance of encased steel stanchions”. Proceedings of the Institution of Civil Engineers - ICE; 27: 77-97, 1964.

[6] Schleich , JB. Computer Assisted analysis of the fire resistance of steel and composite concrete-steel structure,Luxembourg . Final Report EUR 10828 , 1987

[7] Karl Kordina ‘‘Behaviour of Composite Columns and Girders in Fire’’ Technical University of Braunschweig - FIRE SAFETY SCIENCE-PROCEEDINGS OF THE SECOND INTERNATIONAL SYMPOSIUM, pp. 681-695.

[8] Lie TT, Chabot M. ‘‘A method to predict the fire resistance of circular steel columns filled hollow steel columns’’. Journal of Fire Protection Engineering; 2(4):111–26, 1990.

[9] Stefan Winter and Jörg Lange, Behaviour of partially encased composite columns using high-strength steel – ultimate load and fire condition, Leipzig University, Steel and timber structures.

[10] Han LH, Yang YF, Yang H, Huo JS. Residual strength of concrete-filled RHScolumns after exposure to the ISO-834 standard fire. Thin-Walled Structures; 2002;40:991–1012.

[11] Brent Pricket, Robert Driver, "Behaviour of partially encased composite columns made with high performance concrete", Structural Engineering report nº 262, University of Alberta, Department of Civil & Environmental Engineering, 2006.

[12] António J.P. Moura Correia, João Paulo C. Rodrigues Fire resistance of partially encased steel columns with restrained thermal elongation 67 (2011) 593–601.

[13] Shan-Shan Huang, Buick Davison, Ian W. Burgess, High-temperature tests on joints to steel and partially-encased H-section columns, Journal of Constructional Steel Research 80 (2013) 243–251.

[14] Paulo A.G. Piloto, Ana B. R. Gavilan, Marco Zipponi, Alberto Marini, Luís M. R. Mesquita, Giovanni Plizzari; "Experimental Investigation of the Fire Resistance of Partially Encased Beams" journal of Constructional Steel Research Jan2013.

[15] Sadaoui Arezki, Illouli Said , Practical fire design of partially encased composite steel-concrete columns according to Eurocode 4, MATEC Web of Conferences, 11.01029(2014).

[16] "Designing fire safety for steel – recent work", *Proceedings of the ASCE Spring Convention*, American Society of Civil Engineers, New York, 11-15 May, 16pp.

[17] CEN - EN 1991-1-2; "Eurocode 1: Actions on structures - Part 1-2: General actions on structures exposed to fire", European standards; Brussels, 2009.

[18] CEN - EN 1993-1-2; "Eurocode 3: Design of steel structures - Part 1-2: General rules - Structural fire design", *European standards*; Brussels, April 2005.

[19] CEN - EN 1992-1-2; "Eurocode 2: Design of concrete structures - Part 1-2: General rules structural fire design.", *European standards*; Brussels, 2004.

[20] CEN - EN 1992-1-1; “Eurocode 2: Design of concrete structures - Part 1-1: General rules and rules for buildings.”, European standards; Brussels, 2004.

[21] Arezki, S. and I. Said. Practical fire design of partially encased composite steel-concrete columns according to Eurocode 4. International Congress on Materials & Structural Stability, 2014. MATEC Web of Conferences 11, 01029-pp. 1-8.

[22] O. Jungbluth, Optimierte Verbandbauteile, Stahlbau Handbuch 1, Stahlbeau-Verglas-Gmbh, Köeln, 1982.

[23] Paulo Piloto, David Almeida, A. B Ramos-Gavilán, Luís M. R. Mesquita; “Partially Encased Section: Strength and Stiffness Under Fire Conditions”; pp: 15-18, Book of Abstracts of the IFireSS – International Fire Safety Symposium, ISBN 978-989-98435-3-0, pp: 29-38, Book of full papers ISBN 978-989-98435-5-4, ISSN 2412-2629, University of Coimbra, Portugal, 20th-22nd April 2015.

[24] Paulo Piloto, Luís Mesquita, A. B Ramos-Gavilán and David Almeida, “Axial Buckling Load of Partially Encased Columns Under Fire – New Formulae”, X congresso de Construção Metálica e Mista, ISBN 978-989-99226-1-7,pp: II 383 - II 392, Iparque Coimbra, 26-27 de novembro de 2015.

[25] Cajot Louis-Guy, Gallois Louis, Debruyckere Rik, Franssen Jean-Marc, Simplified design method for slim floor beams exposed to fire, Proceedings of the Nordic Steel Construction Conference, Oslo, Norway, 5-7 September, 2012.

[26] R. Zaharia, D. Duma, O.Vassart, Th. Gernay, J.M. Franssen, simplified method for temperature distribution in slim floor beams, Application of Structural Fire Design, Prague, Czech Republic, 29 April 2011.

[27] R. Zaharia and J. M. Franssen, Simple equations for the calculation of the temperature within the cross-section of slim floor beams under ISO Fire, Steel and Composite Structures, Vol.13,No.2(2012)pp171-185.(doi: 10.12989/scs.2012.13.2.171).

[28] ANSYS® Academic Research, Release 16.2, Help System, Element reference, ANSYS, Inc.

[29] Abdelkadir Fellouh, Nourredine Benlakehal, Paulo Piloto, Ana Ramos, Luís Mesquita; Load Carrying Capacity of Partially Encased Columns for Different Fire Ratings, 5th workshop in Urban Fire Safety, Abstract in Book pp: 45-46, Full paper in CD pp: 1-9, Scientific and Technical Division Office, National Laboratory for Civil Engineering (LNEC), Lisbon, Portugal, 1st -2nd June 2016.

This page was intentionally left in blank